MyD88 signalling in B cells and antibody responses during Oropouche virus-induced neurological disease in mice

Daniel Augusto Toledo-Teixeira,[a] Pierina Lorencini Parise,[a] Bruno Brito Pereira da Silva,[a] Camila Lopes Simeoni,[a] Aline Vieira,[a] Julia Forato,[a] Matheus Cavalheiro Martini,[a] Mariene Ribeiro Amorim,[a] Karina Bispo-dos-Santos,[a] Natália Silva Brunetti,[a] Gabriela Fabiano de Souza,[a] Lais Durço Coimbra,[b] Marina Alves Fontoura,[b] Stéfanie Primon Muraro,[a] Priscilla Paschoal Barbosa,[a] Valquíria Aparecida Matheus,[a] Xinyi Hua,[c] Pedro Manoel Mendes de Moraes Vieira,[a] Fabiana Granja,[d] Pritesh Lalwani,[e] Marco Aurélio Ramirez Vinolo,[a,f,g] Guilherme Paier Milanez,[a] Rafael Elias Marques,[b] Ceri Alan Fielding,[h] William Marciel de Souza,[c] Alessandro dos Santos Farias,[a,f,g] David Anthony Price,[h,i] Michael Steven Diamond,[j,k] Eduardo Lani Volpe Silveira,[l,m,*] and José Luiz Proenca-Modena[a,f,m,**]

[a]Department of Genetics, Evolution, Microbiology, and Immunology, Institute of Biology, University of Campinas, Campinas, SP, Brazil
[b]Brazilian Biosciences National Laboratory, Brazilian Centre for Research in Energy and Materials, Campinas, SP, Brazil
[c]Department of Microbiology, Immunology, and Molecular Genetics, University of Kentucky, Lexington, KY, USA
[d]Biodiversity Research Centre, Federal University of Roraima, Boa Vista, RR, Brazil
[e]Instituto Leônidas e Maria Deane, Fiocruz Amazônia, Manaus, AM, Brazil
[f]Experimental Medicine Research Cluster, University of Campinas, Campinas, SP, Brazil
[g]Obesity and Comorbidities Research Centre, University of Campinas, Campinas, SP, Brazil
[h]Division of Infection and Immunity, Cardiff University School of Medicine, University Hospital of Wales, Cardiff, UK
[i]Systems Immunity Research Institute, Cardiff University School of Medicine, University Hospital of Wales, Cardiff, UK
[j]Department of Medicine, Washington University School of Medicine, Saint Louis, MO, USA
[k]Department of Molecular Microbiology, Pathology, and Immunology, Washington University School of Medicine, Saint Louis, MO, USA
[l]Department of Clinical and Toxicological Analyses, School of Pharmaceutical Sciences, University of São Paulo, São Paulo, SP, Brazil

eBioMedicine
2025;117: 105815
Published Online 19 June 2025
https://doi.org/10.1016/j.ebiom.2025.105815

Summary

Background Oropouche virus (OROV) is a neglected insect-borne orthobunyavirus that causes a febrile illness, neurological disease, and pregnancy complications in humans across an endemic area spanning South and Central America. The host factors associated with disease pathogenesis have nonetheless remained obscure, and little is known about the immune determinants of protection against OROV.

Methods We tracked morbidity, mortality, viral loads, and serum neutralisation in wild-type (WT), *Rag1*$^{-/-}$, *CD19*-Cre^{+} *Ifnar*^{fl}, and *CD19*-Cre^{+} *MyD88*^{fl} mice and performed immunophenotyping experiments, passive serum transfers, and adoptive cell transfers to determine how early antibody responses and B cell subsets control viral replication and dissemination to the central nervous system after infection with OROV.

Findings In line with a protective role for B cells, WT mice efficiently produced OROV-specific antibodies within 6 days of infection. Serum transfer containing neutralising IgM from WT to *Rag1*$^{-/-}$ mice prevented neurological disease in OROV-challenged mice. *CD19*-Cre^{+} *MyD88*^{fl} mice but not *CD19*-Cre^{+} *Ifnar*^{fl} mice were vulnerable to neurological disease and produced lower titres of OROV-specific antibodies that exhibited suboptimal neutralisation and potency compared with *MyD88*-sufficient mice. *CD19*-Cre^{+} *MyD88*^{fl} mice also presented with reduced numbers of marginal zone B (MZB) cells and plasmablasts after infection, which were associated with high viral burdens and lethality. Adoptive transfer of MZB cells from WT mice protected *CD19*-Cre^{+} *MyD88*^{fl} mice and partially protected *Rag1*$^{-/-}$ mice from lethal infection with OROV.

Interpretation Early MyD88 signalling in B cells is required for optimal antibody responses that limit viral replication and neurological disease in mice infected with OROV.

Funding São Paulo Research Foundation (FAPESP), National Council for Scientific and Technological Development (CNPq), Coordination for the Improvement of Higher Education Personnel (CAPES), Unicamp Research Affairs

*Corresponding author. School of Pharmaceutical Sciences, University of São Paulo, 580 Professor Lineu Prestes Ave., Building 17, São Paulo, SP 05508-000, Brazil.
**Corresponding author. Institute of Biology, University of Campinas, 255 Monteiro Lobato St., E1 Second Floor, Campinas, SP 13083-862, Brazil.
E-mail addresses: eduardosilveira@usp.br, elvsilveira@gmail.com (E.L.V. Silveira), jlmodena@unicamp.br, jlmodena@gmail.com (J.L. Proenca-Modena).
[m]Senior authors contributed equally.

Office, PIPAE University of São Paulo, Wellcome Trust, and National Institute of Science and Technology on Photonics Applied to Cell Biology (INFABIC, Unicamp).

Keywords: Oropouche virus; Marginal zone B cells; Innate immune response; IgM; Emerging viruses; Vector-borne diseases

Research in context

Evidence before this study

Oropouche virus (OROV) is a neglected arbovirus transmitted to humans living mainly in the Amazon basin after inoculation by *Culicoides paraensis*. It is currently responsible for an emerging outbreak of fever and encephalitis across several countries in South and Central America. Early antibody responses are thought to limit viral replication and prevent disease, but few studies have addressed this issue directly, and little is known about the role of B cell subsets as mediators of protection against OROV.

Added value of this study

We demonstrate that B cells but not T cells are essential for immune control of OROV in mice. In particular, we show that early antibody responses are produced mainly by marginal zone B cells in a MyD88-dependent manner and restrict viral replication and spread to the central nervous system, protecting mice from encephalitis and subsequent death.

Implications of all the available evidence

Our findings suggest that MyD88 signalling in B cells is required for optimal antibody responses that protect mice against the severe neurological disease manifestations of OROV. These results could facilitate the development of antibody treatment strategies and vaccines to mitigate future outbreaks of OROV.

Introduction

Oropouche virus (OROV) is a vector-borne orthobunyavirus that is endemic in Latin America and the Caribbean and has been estimated to cause more than half a million cases in multiple outbreaks since 1960.[1–4] OROV is currently spreading rapidly beyond its traditional confines in the Amazon region, with a substantial increase in the number of expected infections from November 2023 to June 2024 and from October 2024 to April 2025.[5] Autochthonous cases have recently been documented outside Amazonia, extending to Colombia, Peru, Bolivia, and Cuba.[6–8] OROV nonetheless remains a largely neglected pathogen.[3,9]

OROV is a trisegmented negative single-stranded RNA virus classified as *Orthobunyavirus oropoucheense* in the family *Peribunyaviridae* and the order *Bunyavirales*.[10,11] Genetic reassortment is a feature of OROV and underlies the current outbreak.[6,12] OROV is maintained in a sylvatic cycle among amplifier hosts, including sloths and potentially other vertebrates, such as nonhuman primates, migratory birds, and rodents.[10,13–15] Humans are dead-end hosts, and *Culicoides paraensis* is the main vector in the urban cycle. Other mosquitoes, notably *Aedes serratus* and *Culex quinquefasciatus*, can also transmit OROV.[1,10,13–15]

OROV infection causes an acute febrile illness in humans that is associated with headache, myalgia, arthralgia, photophobia, polyuria, and skin rash.[16] Most symptoms last for approximately one week, although in many cases, symptoms can persist and relapse.[15–17] The virus has been detected in peripheral blood leukocytes isolated from patients[18] and can infect human peripheral blood mononuclear cells *in vitro*.[19] OROV infection can be lethal and has also been linked with foetal abnormalities and abortion as well as neurological disease in unborn children[20–22] and adults resulting from invasion of the central nervous system (CNS).[3,16,23–25] The underlying mechanisms of neuroinvasion and neuropathogenesis nonetheless remain obscure.

Many arboviral infections trigger type I interferon (IFN) responses in vertebrates, inducing the expression of IFN-stimulated genes (ISGs) that collectively hinder viral replication.[26,27] A previous study demonstrated that *Ifnar*$^{-/-}$ mice, which lack the IFN-α/β receptor, and *Irf3/5/7*$^{-/-}$ mice, which lack IFN regulatory factors (IRFs) 3, 5, and 7, succumb to OROV infection.[28] However, *Irf3/7*$^{-/-}$ mice, which lack IRF3 and IRF7 but retain IRF5, were less vulnerable to viral challenge than *Irf5*$^{-/-}$ mice.[28] These latter mice exhibited signs of neurological disease and died from the infection, a susceptibility associated with lower titres of virus-specific neutralising antibodies compared with OROV-infected wild-type (WT) mice.[28] IRF5 is constitutively expressed in haematopoietic cells, including B cells,[29,30] where it regulates the expression of B lymphocyte-induced maturation protein-1 (Blimp-1 or PRDM1),[31,32] which demarcates antibody production. These observations suggest that B cell responses can contribute to

protection against OROV-mediated neurological disease. In the present study, we investigated this hypothesis in mice.

Methods

Ethics

All animal procedures were performed in compliance with ARRIVE guidelines 2.0 (https://arriveguidelines.org/arrive-guidelines) and approved by the University of Campinas (Unicamp) Ethics Committee on Animal Use (protocol numbers 4876-1, 5181-1, and 5459-1).

Mice

C57BL/6 WT mice (RRID:MGI:7264313) were obtained from the Multidisciplinary Centre for Biological Research (Unicamp), C57BL/6 *Rag1*$^{-/-}$ mice (RRID:MGI:2163461) were kindly donated by Prof. Dr. Jean Pierre Schatzmann Peron (University of São Paulo), C57BL/6 *CD19*-Cre^{+} (RRID:IMSR_JAX:006785) and C57BL/6 *MyD88*^{fl} mice (RRID:MGI:3829502) were kindly provided by Prof. Dr. Niels Olsen Câmara (University of São Paulo), and C57BL/6 μMT (RRID:IMSR_JAX:002288), C57BL/6 TCRβδ (RRID:IMSR_JAX:002122), and C57BL/6 *Ifnar*^{fl} mice (RRID:IMSR_JAX:028256) were purchased from The Jackson Laboratory. Mouse strains were maintained with *ad libitum* access to food and water and were manipulated in the Biosafety Level 2 Specific Pathogen-Free Facility at the Department of Genetics, Evolution, Microbiology, and Immunology at the Institute of Biology (Unicamp). No exclusion criteria were applied during this study. Mouse group sizes were determined using power analyses (alpha = 0.05) as described previously.[28] To achieve 80% power for the detection of a 1.0 $\log_{10}$ change, three mice were required per group based on an expected standard deviation of 0.3 $\log_{10}$, and five mice were required per group based on an expected standard deviation of 0.5 $\log_{10}$. Accordingly, at least three mice were included per group in each experiment, except for some noncritical groups, and each experiment was performed at least twice independently. Male and female mice were used in all experiments, and sex was not considered as a biological variable. The number of mice used in each experiment is described in the relevant legend for each figure.

Virus and cell lines

OROV strain BeAn19991 (RRID:NCBITaxon_118655) was kindly provided by Prof. Dr. Luiz Tadeu Morais Figueiredo (University of São Paulo) and propagated in Vero cells at the Laboratory of Emerging Viruses (Unicamp). Vero cells were purchased directly from the ATCC (CCL-81, RRID:CVCL_0059) and cultured in Dulbecco's Modified Eagle Medium (DMEM, Sigma–Aldrich) supplemented with 5% heat-inactivated foetal bovine serum (FBS, Gibco), 100 IU/mL penicillin (Sigma–Aldrich), and 100 μg/mL streptomycin (Sigma–Aldrich). Virus stocks and cell lines routinely tested negative for mycoplasma by PCR.[33]

Virus infection and sample acquisition

Mice were sedated and inoculated with 10^5 focus-forming units (FFU) of OROV delivered subcutaneously into the left posterior plantar footpad in a final supernatant volume of 50 μL. An identical volume of supernatant derived from uninfected Vero cells was used as a negative control in all experiments. Mice were randomly allocated and housed separately for each condition, irrespective of initial weight and sex. After infection, mice were monitored daily for 21 days and individually assigned to clinical scores as follows: (1) active animal, no disease; (2) slow walking, slightly closed eyes, or slight impairment of balance; (3) apathy, ataxia, closed eyes, severe impairment of balance, circular walking, lethargy, or paralysis; or (4) moribund or deceased animal. Mice assigned to clinical scores 3 or 4 were euthanised immediately with an isoflurane overdose. Other mice were euthanised similarly on day 21 post-infection. These time points were defined as the terminal harvest in each case. Blood was collected via cardiac puncture for terminal harvesting or via the retro-orbital sinus for repeated harvesting after sedation. Dissection for organ collection was performed in a laminar flow cabinet after perfusion with 20 mL of 0.15 M phosphate-buffered saline (PBS, pH 7.4). Serum was obtained after centrifugation of clotted blood at 12,000 × *g* for 15 min at 4 °C. Organs were homogenised with zirconium beads for 40 s at 6000 rpm in 1 mL of DMEM supplemented with 5% FBS (Gibco), 100 IU/mL penicillin (Sigma–Aldrich), and 100 μg/mL streptomycin (Sigma–Aldrich) using a MagNA Lyser Instrument (Roche). All samples were stored at −80 °C. Investigators were aware of group allocations during experimentation.

Virus titration

Mouse samples and cell supernatants were thawed and clarified via centrifugation at 12,000 × *g* for 15 min at 4 °C. The clarified supernatants were serially diluted and added to Vero-E6 cells (CRL-1586, RRID:CVCL_0574) seeded in 96-well plates (Corning). After 2 h, semisolid medium comprising DMEM supplemented with 5% FBS (Gibco), 100 IU/mL penicillin (Sigma–Aldrich), 100 μg/mL streptomycin (Sigma–Aldrich), and 0.75% medium-viscosity carboxymethylcellulose sodium (Sigma–Aldrich) was added to the cultures, and after further 36 h, cells were fixed in 4% paraformaldehyde (pH 9.6, Sigma–Aldrich) overnight at 4 °C. Cells were then washed with PBS. Nonspecific antigens were blocked via incubation with 5% skimmed milk powder (Molico) dissolved in PBS for 30 min at room temperature. Cells were washed between incubations with PBS containing 0.1% bovine serum albumin (BSA) and 0.1% Triton X-100. OROV polyclonal

immune ascitic fluid (VR-1228AF, ATCC) diluted 1:1000 in 5% skimmed milk powder was added first for 2 h at room temperature. Cells were then washed and incubated with goat anti-mouse peroxidase-conjugated IgG (Sigma–Aldrich #A4416, RRID:AB_258167) diluted 1:2000 in 5% skimmed milk powder for 1 h at room temperature. Cells were then washed again and incubated with TrueBlue Peroxidase Substrate (KPL). Foci were counted visually.

RNA extraction and quantification

Tissue RNA was extracted via the phenol-chloroform method using TRIzol (Invitrogen) and further purified using a PureLink RNA Mini Kit (Invitrogen). All eluted samples were quantified using a Nanodrop One Spectrophotometer (Thermo Fisher Scientific). OROV RNA was measured in tissues via RT-qPCR using TaqMan Fast Virus 1-Step Master Mix (Applied Biosystems).[18]

Focus reduction neutralisation test (FRNT)

Serum samples were inactivated by heating at 56 °C for 30 min and diluted 2-fold initially and then 4-fold serially in DMEM supplemented with 100 IU/mL penicillin (Sigma–Aldrich) and 100 μg/mL streptomycin (Sigma–Aldrich). OROV polyclonal immune ascitic fluid (VR-1228AF, ATCC) was used as a positive control for neutralisation. Samples were mixed via homogenisation in equal volumes with 100 FFU of OROV. Virus titration was performed as described above. $FRNT_{50}$ values were defined via theoretical sample dilution to 50% reduction of infectivity versus positive controls using a three-parameter log-logistic regression curve fit.

ELISAs and Luminex

OROV-specific antibodies were quantified using an in-house ELISA. Plates were coated with 10^5 FFU of OROV in 100 mM carbonate-bicarbonate buffer (pH 9.6) overnight at 4 °C. After washing five times with washing buffer (PBS containing 0.05% Tween-20), plates were incubated with blocking buffer (washing buffer containing 10% skimmed milk powder) for 30 min at 37 °C. Serum samples were diluted 10-, 50-, 100-, and 200-fold in blocking buffer and added to the plates for 2 h at 37 °C. For the avidity assay, paired samples were incubated with 6 M urea for 10 min at 37 °C. After washing five times with washing buffer, goat anti-mouse peroxidase-conjugated IgM (Abcam #ab97230, RRID:AB_10688258) or goat anti-mouse peroxidase-conjugated IgG (Abcam #ab6789, RRID:AB_955439), respectively diluted 1:5000 or 1:10,000 in blocking buffer, was added for 1 h at 37 °C. Plates were then washed again five times with washing buffer and incubated with 3,3',5,5'-tetramethylbenzidine (Sigma–Aldrich) for 30 min at room temperature in a dark chamber before reading at 650 nm using an Epoch Spectrophotometer (BioTek). IFN-α was quantified using a VeriKine Mouse Interferon-Alpha ELISA Kit (PBL Assay Science), and IFN-β was quantified using a Mouse IFN-Beta DuoSet ELISA Kit (R&D Systems). Levels of IFN-γ, IL-1β, IL-6, IL-10, IL-12, CXCL1, GM-CSF, and TNFα were determined using a Mouse Magnetic Luminex Assay Kit (R&D Systems).

Passive transfer studies

Serum was transferred to sedated *Rag1*$^{-/-}$ mice via tail vein injection. IgM content was chemically depleted via incubation with an equal volume of 0.05 M β-mercaptoethanol (β-ME, Sigma–Aldrich) diluted in PBS for 1 h at 37 °C. Negative controls comprised β-ME diluted in PBS. Mice were randomly allocated and housed separately for each condition, irrespective of initial weight and sex.

Morphological analysis of brain tissues

Brain tissues were fixed in 4% paraformaldehyde (Sigma–Aldrich) for 24 h at room temperature. After washing four times with distilled water, each for 10 min, tissues were maintained in 70% ethanol until inclusion in paraffin. Histological sections were cut at a thickness of 5 μm and stained with haematoxylin and eosin. Images were acquired using an Eclipse Ts2 Microscope (Nikon).

Immunofluorescence microscopy of brain tissues

Brain tissues were fixed in 4% paraformaldehyde (Sigma–Aldrich) for 1 h at room temperature. After washing three times with PBS, each for 20 min, tissues were soaked in 15% sucrose diluted in PBS and incubated overnight at 4 °C. Tissues were then soaked in 30% sucrose diluted in PBS and maintained at 4 °C. Sections were taken from the coronal plane at the posterior region of the diencephalon, soaked in optimal cutting temperature (OCT) compound at −70 °C with liquid nitrogen-cooled *n*-hexane, cut at a thickness of 5 μm in a Leica Biosystems Cryostat (CM1860 UV), and maintained at −80 °C. Sections were then washed with PBS, blocked with a blocking solution (PBS containing 5% BSA and 0.1% Tween-20) for 1 h at room temperature, and incubated with OROV polyclonal immune ascitic fluid (VR-1228AF, ATCC) diluted 1:500 in PBS containing 3% BSA overnight at 4 °C. After washing with PBS, sections were incubated with goat anti-mouse FITC-conjugated IgG (Sigma–Aldrich #F5262, RRID:AB_259638) diluted 1:1000 in PBS containing 1% BSA for 2 h at room temperature, washed again with PBS, and incubated with rabbit anti-ionised calcium-binding adaptor molecule 1 (IBA1, Fujifilm Wako #019-19741, RRID:AB_839504) diluted 1:500 in PBS containing 3% BSA overnight at 4 °C. Sections were then washed again with PBS, incubated with goat anti-rabbit Cy3.5-conjugated IgG (Abcam #ab6941, RRID:AB_955037) diluted 1:1000 in PBS containing 1% BSA for 2 h at room temperature, and washed a final time with PBS. Slides were prepared using ProLong Gold

Antifade Mountant with DAPI (Thermo Fisher Scientific). Images were acquired using an Upright LSM780-NLO Confocal Microscope (Zeiss) at the National Institute of Science and Technology on Photonics Applied to Cell Biology (INFABIC, Unicamp).

Flow cytometry

OROV-infected splenocytes were labelled with Fixable Viability Stain 510 (BD Horizon) for 30 min at 4 °C. Cells were then washed with PBS, fixed in 4% paraformaldehyde (Sigma–Aldrich) for 30 min at 4 °C, and analysed using a FACSCelesta (BD Biosciences). For immunophenotyping, splenocytes from OROV-infected and uninfected mice were harvested on days 6 or 14 after infection or mock manipulation, counted, and stained with combinations of the following antibodies for 30 min at 4 °C in a dark chamber: anti-B220–APC-Cy7 (0.4 μg/sample, clone RA3-6B2, BioLegend #103223, RRID:AB_313006), anti-CD3–FITC (1.0 μg/sample, clone 17A2, BioLegend #100204, RRID:AB_312661), anti-CD23–PE-Cy7 (0.4 μg/sample, clone B3B4, BioLegend #101614, RRID:AB_2103036), anti-CD38–APC (0.1 μg/sample, clone 90, BioLegend #102711, RRID:AB_312932), anti-CD138–PE (0.4 μg/sample, clone 281-2, BioLegend #142504, RRID:AB_10916119), anti-F4/80–FITC (0.5 μg/sample, clone BM8, BioLegend #123107, RRID:AB_893500), anti-GL7–PerCP-Cy5.5 (0.2 μg/sample, clone GL7, BioLegend #144609, RRID:AB_2562978), and anti-Gr1–FITC (0.5 μg/sample, clone RB6-8C5, BioLegend #108406, RRID:AB_313371). Data were acquired using an LSRFortessa (BD Biosciences).

Adoptive cell transfer studies

$B220^{hi}$ $CD23^{-}$ marginal zone B (MZB) cells were purified from the spleens of WT or *CD19*-Cre^{+} $MyD88^{fl}$ mice via flow cytometry using a FACSMelody (BD Biosciences). Each sedated $Rag1^{-/-}$ or *CD19*-Cre^{+} $MyD88^{fl}$ mouse received 5×10^{5} MZB cells via retro-orbital sinus injection. After 24 h, mice were inoculated with OROV and monitored as described above. Mice were randomly allocated and housed separately for each condition, irrespective of initial weight and sex.

Factor analysis of mixed data (FAMD)

IgM and IgG quantity, avidity, and neutralisation potency (indices and $FRNT_{50}$ values), brain viral loads, mortality, and the cellularity of B cell populations from WT and *CD19*-Cre^{+} $MyD88^{fl}$ mice were used for FAMD. All paired data were available for mice succumbing to OROV infection with a clinical score >1. Other data were randomly paired among WT or *CD19*-Cre^{+} $MyD88^{fl}$ mice.

Statistics

Data were analysed using Prism version 8 (GraphPad Software). Normality distributions were assessed using the Shapiro–Wilk test. Comparisons across three or more groups were performed using the Kruskal–Wallis test with Dunn's post-hoc test or the Mann–Whitney test with Bonferroni correction for group pairs. Survival curves were compared using a log-rank test with Bonferroni correction. FAMD was performed using R project version 4.1.1[34] with packages *FactoMineR* version 2.4[35] and *factoextra* version 1.0.7.[36] $FRNT_{50}$ values were calculated using the same version of R with the *dcr* package.[37] Relative gene expression was calculated using the ΔΔCq method. Flow cytometry data were analysed using FlowJo version 9.9.3 (FlowJo LLC) with the UMAP[38] and FlowSOM PlugIns.[39] Hypothesis testing for each experiment is described in the relevant legend for each figure. Significance was assigned at $p \leq 0.05$.

Role of funders

The funders had no role in study design, data collection, data analysis, data interpretation, preparation of the manuscript, or the decision to publish.

Results

$Rag1^{-/-}$ mice are vulnerable to OROV infection

OROV-induced disease is age-dependent in different strains of mice. Newborn C57BL/6, BALB/c, and SJL WT mice die from viral encephalitis, whereas adult mice are not susceptible.[40] To determine whether B and/or T cells are required for protection, we evaluated weight loss, morbidity, and mortality in $Rag1^{-/-}$ mice aged 4–6 weeks or 9–12 weeks after subcutaneous footpad inoculation with OROV. $Rag1^{-/-}$ mice succumbed to infection with median survival times of 16 and 13 days in the younger and older groups, respectively ($p < 0.0001$ in each case versus WT mice, log-rank test with Bonferroni correction), with disease characterised by weight loss and increasing clinical severity (Fig. 1a–c). Signs of neurological damage, including lethargy, paralysis, and ataxia, were detected after day 7 of viral inoculation. All further experiments were performed using mice aged 4–6 weeks.

OROV replicates at high titres in the brains and spinal cords of $Rag1^{-/-}$ mice

To determine the basis of susceptibility to OROV infection in the absence of adaptive immune responses, we quantified viral loads in the serum, inguinal lymph nodes, liver, spleen, kidneys, brain, and spinal cord of individual WT or $Rag1^{-/-}$ mice on days 1, 3, 6, and 14 after infection or at terminal harvest using a focus-forming assay and RT-qPCR. As expected from our previous work,[40] we did not recover infectious OROV from any site in WT mice. However, OROV RNA was detected at low levels in several tissues, including the brain and spinal cord, isolated from WT mice (Fig. 1d–j). In contrast, all $Rag1^{-/-}$ mice exhibited viraemia after day 1 post-infection, and infectious virus particles and

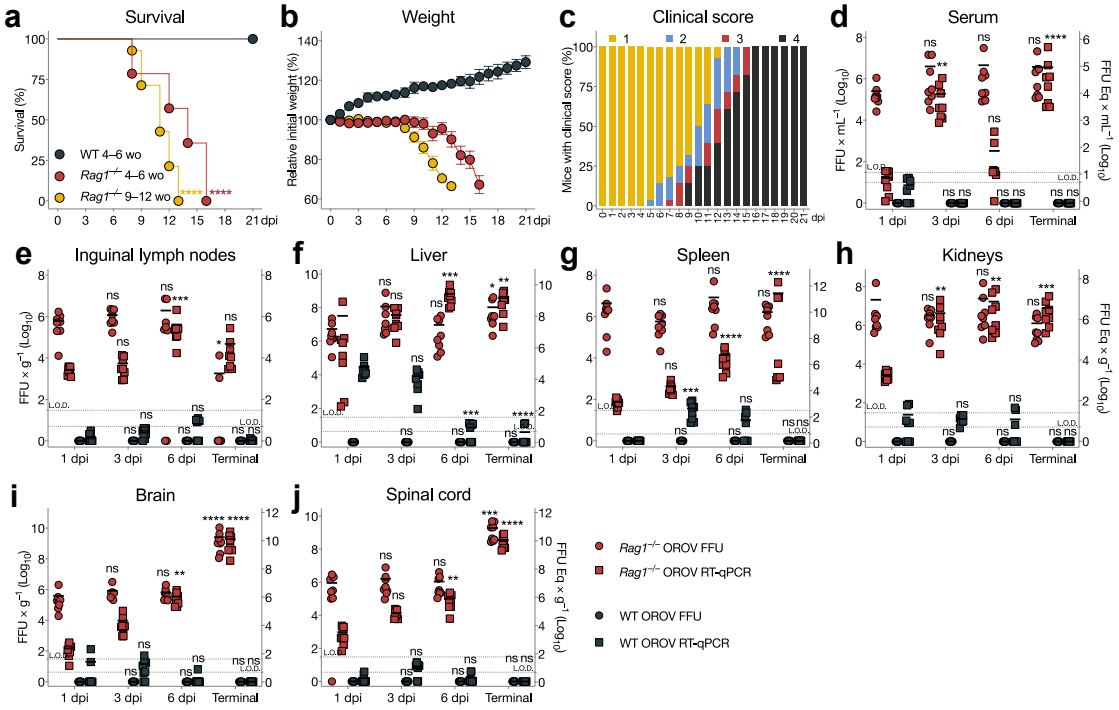

***Fig. 1:* Mortality, weight loss, morbidity, and viral loads for *Rag1*$^{-/-}$ mice after OROV infection.** (a) Survival and (b) weight of C57BL/6 WT mice aged 4–6 weeks (grey, $n = 14$), *Rag1*$^{-/-}$ mice aged 4–6 weeks (red, $n = 14$), and *Rag1*$^{-/-}$ mice aged 9–12 weeks (orange, $n = 14$) over 21 days post-infection (dpi) with 10^5 FFU of OROV. Statistical differences were assessed using a log-rank test with Bonferroni correction (a). ****$p < 0.0001$. (c) Clinical scores for *Rag1*$^{-/-}$ mice aged 4–6 weeks ($n = 14$) after OROV infection. Bars indicate the percent occurrence for each clinical score among all mice. Clinical scores were defined as follows: (1) active animal, no disease; (2) slow walking, slightly closed eyes, or slight impairment of balance; (3) apathy, ataxia, closed eyes, severe impairment of balance, circular walking, lethargy, or paralysis; or (4) moribund or deceased animal. (d–j) Viral loads in serum and tissues from infected *Rag1*$^{-/-}$ mice (red, $n = 8$ at each time point) and WT mice (grey, $n = 8$ at each time point) measured via focus-forming assay (circles correspond to left y-axis) or RT-qPCR (squares correspond to right y-axis). Statistical differences were assessed using the Kruskal–Wallis test with Dunn's post-hoc test for each group versus day 1 post-infection. *$p < 0.05$, **$p < 0.01$, ***$p < 0.001$, ****$p < 0.0001$, ns = not significant. Symbols represent death events (a), mean ± SEM (b), or individual viral loads (d–j), and lines represent mean values (d–j). Data were pooled from at least three independent experiments. FFU Eq = focus-forming unit equivalents; L.O.D. = limit of detection.

OROV RNA were recovered from all sites at different time points after inoculation (Fig. 1d–j). We also detected OROV antigens in brain sections from *Rag1*$^{-/-}$ mice at terminal harvest via indirect immunofluorescence microscopy (Supplemental Fig. S1). Neuronal-shaped cells frequently stained positive for OROV (Supplemental Fig. S1). Moreover, discrete staining was observed for IBA1, indicating microglial activation (Supplemental Fig. S1).[40,41] No further morphological brain alterations were identified via staining with haematoxylin and eosin. Infectious viral loads in the CNS were increased by more than two orders of magnitude at the time of death between days 8 and 16 ($p < 0.0001$ versus day 1, Kruskal–Wallis test with Dunn's post-hoc test), indicating persistent infection (Fig. 1i and j). These data suggested that B and/or T cells were essential for restricting OROV infection and dissemination into the CNS.

B cells are required to control OROV infection

As *Rag1*$^{-/-}$ mice lack mature B and T cells,[42] we investigated the roles of these cell lineages as mediators of immune protection against OROV by assessing morbidity and mortality in μMT and TCRβδ mice, which lack mature B or T cells, respectively.[43,44] WT and TCRβδ mice were resistant to disease caused by OROV infection, whereas μMT mice died 1–3 weeks after viral challenge ($p < 0.0001$ for μMT mice versus WT or TCRβδ mice, log-rank test with Bonferroni correction) (Fig. 2a). OROV-infected μMT mice developed severe disease, exhibiting weight loss, lethargy, ataxia, and limb paralysis close to the day of death (Fig. 2b and c), and high titres of OROV were recovered from various organs and serum (Fig. 2d–j). These observations indicated that B cells but not T cells were required to restrict OROV infection.

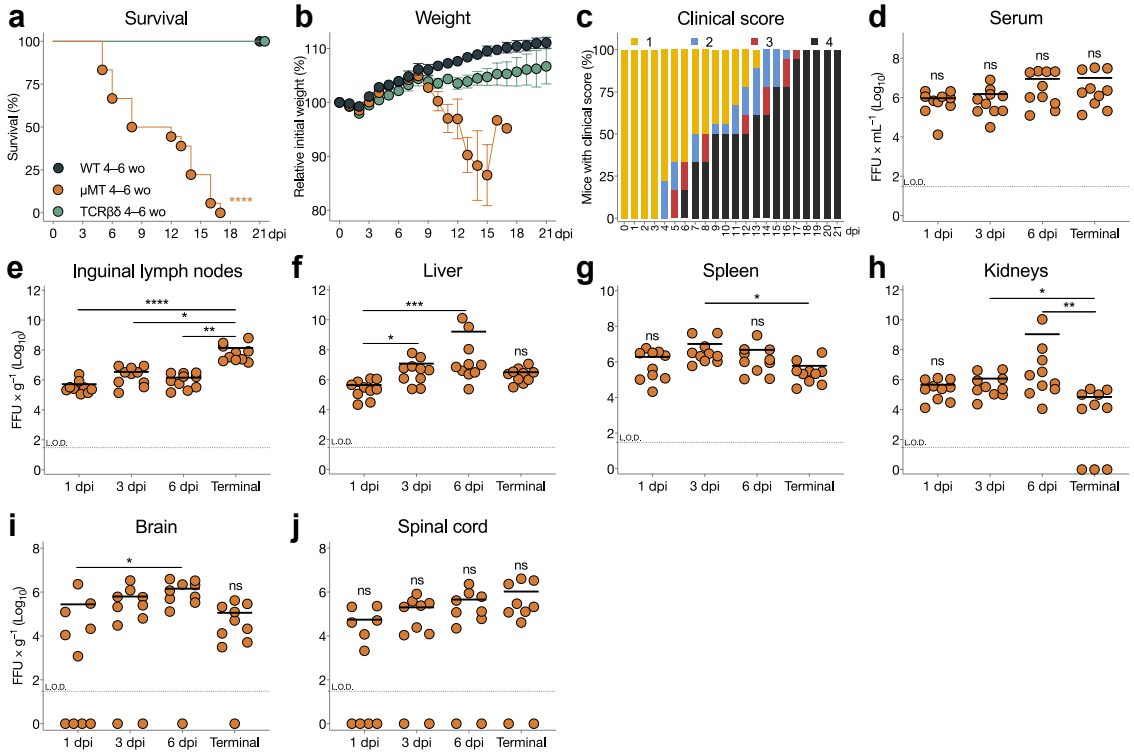

***Fig. 2:* Mortality, weight loss, morbidity, and viral loads for µMT mice after OROV infection.** (a) Survival and (b) weight of C57BL/6 WT mice (grey, n = 14), µMT mice (orange, n = 18), and TCRβδ mice (green, n = 21) over 21 days post-infection (dpi) with 10^5 FFU of OROV. Statistical differences were assessed using a log-rank test with Bonferroni correction (a). ****$p < 0.0001$. (c) Clinical scores for µMT mice (n = 18) after OROV infection. Bars indicate the percent occurrence for each clinical score among all mice. Clinical scores were defined as in Fig. 1. (d–j) Viral loads in serum and tissues from infected µMT mice (n = 10 at each time point) measured via focus-forming assay. Statistical differences were assessed using the Kruskal–Wallis test with Dunn's post-hoc test across all days post-infection. *$p < 0.05$, **$p < 0.01$, ***$p < 0.001$, ****$p < 0.0001$, ns = not significant. Symbols represent death events (a), mean ± SEM (b), or individual viral loads (d–j), and lines represent mean values (d–j). Data were pooled from at least three independent experiments. L.O.D. = limit of detection.

IFNAR signalling in B cells is not required to control OROV infection

Type I IFNs can restrict several arboviral infections via different mechanisms, and B cells can act as an important source of type I IFNs.[22,45,46] To determine whether type I IFN signalling in B cells is important for controlling OROV infection, we generated *CD19*-Cre$^+$ *Ifnar*$^{fl/fl}$, *CD19*-Cre$^+$ *Ifnar*$^{fl/wt}$, *CD19*-Cre$^+$ *Ifnar*$^{wt/wt}$, and Cre$^-$*Ifnar*$^{fl/fl}$ mice. All of these mice were resistant to OROV infection, exhibiting no weight loss, no signs of disease, and no evidence of uncontrolled viral replication (Supplemental Fig. S2). These results demonstrated that type I IFN signalling in B cells was not required to control OROV infection.

MyD88 signalling in B cells is required to control OROV infection

In an earlier study, we observed that moribund *Irf5*$^{-/-}$ mice exhibited lower systemic neutralising antibody titres than healthy OROV-infected WT mice.[28] IRF5 is a transcription factor associated with B cell maturation that is activated via MyD88 signalling and Toll-like receptors (TLRs).[47–49] To investigate the role of MyD88 signalling in B cells during OROV infection, we generated *CD19*-Cre$^+$ *MyD88*$^{fl/fl}$, *CD19*-Cre$^+$ *MyD88*$^{fl/wt}$, *CD19*-Cre$^+$ *MyD88*$^{wt/wt}$, and Cre$^-$*MyD88*$^{fl/fl}$ mice. Some mice with decreased or no *MyD88* expression in B cells (*CD19*-Cre$^+$ *MyD88*$^{fl/fl}$ and *CD19*-Cre$^+$ *MyD88*$^{fl/wt}$, termed here *CD19*-Cre$^+$ *MyD88*^{fl}) developed weight loss and signs of neurological disease and died after inoculation with OROV ($p < 0.05$ for *CD19*-Cre$^+$ *MyD88*^{fl} mice versus *CD19*-Cre$^+$ *MyD88*$^{wt/wt}$ and Cre$^-$*MyD88*$^{fl/fl}$ mice, log-rank test with Bonferroni correction) (Fig. 3a–d). These phenotypes were associated with high levels of viraemia and viral replication in peripheral organs and the CNS (Fig. 3e–k). *CD19*-Cre$^+$ *MyD88*^{fl} mice with higher clinical scores succumbed to the infection (Fig. 3d). OROV antigens were detected in brain sections from these mice at terminal harvest via indirect immunofluorescence microscopy (Supplemental Fig. S1). In brain sections from neurologically affected mice, neuronal-shaped cells frequently stained positive for

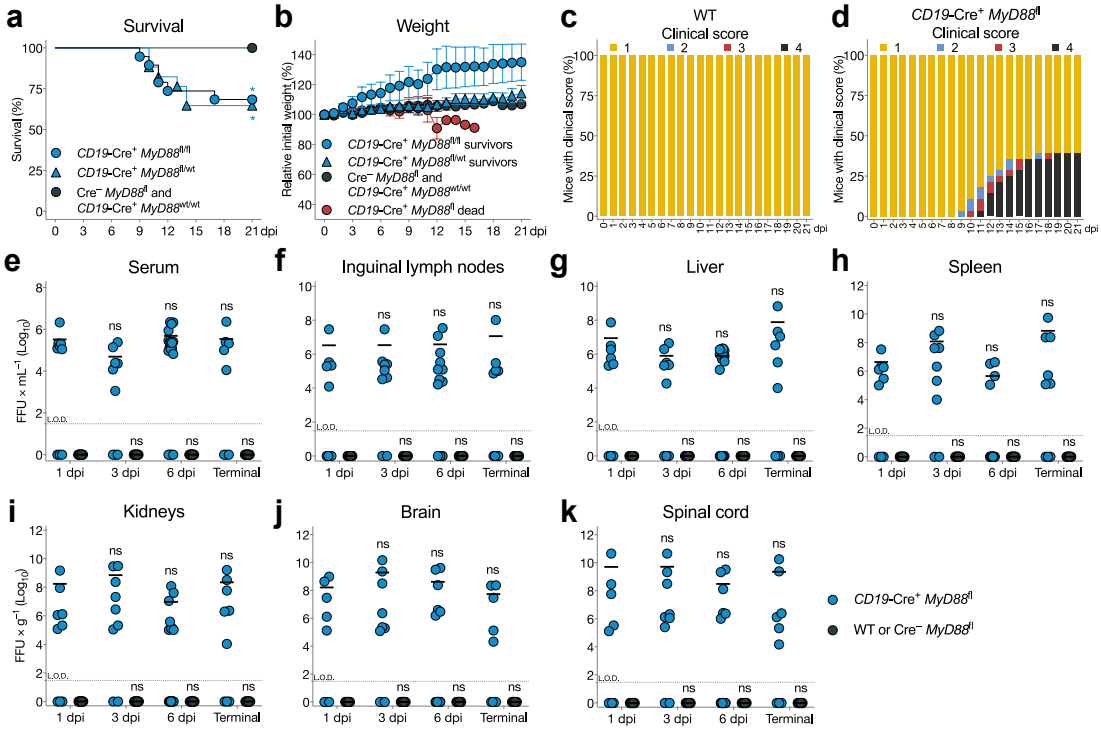

***Fig. 3*: Mortality, weight loss, morbidity, and viral loads for *CD19*-Cre^{+} *MyD88*^{fl} mice after OROV infection.** (a) Survival and (b) weight of *CD19*-Cre^{+} *MyD88*$^{fl/fl}$ mice (blue circles, n = 19), *CD19*-Cre^{+} *MyD88*$^{fl/wt}$ mice (blue triangles, n = 11), and Cre^{-}*MyD88*$^{fl/fl}$ or *CD19*-Cre^{+} *MyD88*$^{wt/wt}$ mice (grey circles, n = 17) over 21 days post-infection (dpi) with 10^5 FFU of OROV. Statistical differences were assessed using a log-rank test with Bonferroni correction (a). *$p < 0.05$. (c, d) Clinical scores for WT mice (n = 19) and *CD19*-Cre^{+} *MyD88*^{fl} mice (n = 19) after OROV infection. Bars indicate the percent occurrence for each clinical score among all mice. Clinical scores were defined as in Fig. 1. (e–k) Viral loads in serum and tissues from infected *CD19*-Cre^{+} *MyD88*^{fl} mice (blue, n = 12 at each time point) and Cre^{-}*MyD88*$^{fl/fl}$ or *CD19*-Cre^{+} *MyD88*$^{wt/wt}$ mice (grey, n = 12 at each time point) measured via focus-forming assay. Statistical differences were assessed using the Kruskal–Wallis test with Dunn's post-hoc test for each group versus day 1 post-infection. ns = not significant. Symbols represent death events (a), mean ± SEM (b), or individual viral loads (e–k), and lines represent mean values (e–k). Data were pooled from at least three independent experiments. L.O.D. = limit of detection.

OROV, and discrete staining was observed for IBA1 (Supplemental Fig. S1). Brain sections from mice lacking overt signs of neurological disease exhibited weaker staining for OROV and IBA1 (Supplemental Fig. S1). No further morphological alterations were identified via staining with haematoxylin and eosin. In contrast, no evidence of ongoing viral replication or signs of disease were observed in control mice (Cre^{-}*MyD88*$^{fl/fl}$ or *CD19*-Cre^{+} *MyD88*$^{wt/wt}$). These results indicated that MyD88 signalling in B cells was required to control OROV infection.

A lack of B and T cells or *MyD88* expression in B cells does not hamper the production of chemokines and cytokines after OROV infection

As the type I IFN response in B cells was not required to control OROV infection, we quantified inflammatory chemokines and cytokines via ELISA and Luminex. Several inflammatory mediators were not detected in serum samples from infected mice, including IFN-γ, IL-6, GM-CSF, and TNF-α. We nonetheless found that WT and Cre^{-}*MyD88*$^{fl/fl}$, *CD19*-Cre^{+} *MyD88*^{fl}, and *Rag1*$^{-/-}$ mice produced IFN-α, IFN-β, IL-1β, IL-10, IL-12 p70, and CXCL1, albeit with no common profiles after infection with OROV (Supplemental Fig. S3).

OROV infection induces high titres of neutralising antibodies in WT mice

To extend these findings, we quantified neutralising antibodies in the serum of OROV-infected WT mice. High titres of neutralising antibodies were detected 14 days after infection, with $FRNT_{50}$ values ≥ 1:65,000 ($p < 0.0001$ versus uninfected WT mice, Kruskal–Wallis test with Dunn's post-hoc test) (Supplemental Fig. S4a and b). Naive WT mice also exhibited some neutralising capacity, potentially due to natural antibodies, with $FRNT_{50}$ values ≥ 1:64 ($p < 0.0001$ versus infected WT

mice, Kruskal–Wallis test with Dunn's post-hoc test) (Supplemental Fig. S4a and b).

Natural antibodies do not substantially restrict OROV neuropathogenesis

Natural antibodies play a key role in controlling infectious agents in mice.[50,51] To investigate this phenomenon in the context of OROV infection, we pooled sera harvested from naive WT mice 14 days after vehicle inoculation (Supplemental Fig. S4a and b) and transferred 100 μL or 400 μL intravenously to *Rag1*$^{-/-}$ mice on the day of viral challenge. Recipient mice exhibited weight loss and developed neurological disease, with high viral loads in peripheral organs and the CNS, and died from the infection (Supplemental Fig. S4c–e). These findings indicated that natural antibodies at the doses administered here were not sufficient to confer immune protection against OROV.

Neutralising antibodies against OROV protect susceptible mice

In further experiments, we pooled sera harvested from WT mice on day 14 after infection (Supplemental Fig. S4a and b) and transferred 100 μL to *Rag1*$^{-/-}$ mice on days 0, 3, or 6 after OROV challenge. Sera transferred within 3 days of challenge protected *Rag1*$^{-/-}$ mice. In contrast, sera transferred after 6 days post-challenge were not protective, as recipient *Rag1*$^{-/-}$ mice developed neurological signs of disease associated with high viral titres in peripheral organs and the CNS (Supplemental Fig. S4f–h). These data revealed that neutralising antibodies could protect against OROV-induced disease if administered early after viral exposure.

OROV neuropathogenesis is restricted by early IgM antibody production

Antibody isotypes are differentially produced in response to antigenic stimuli *in vivo*.[52,53] In mice, virus-specific IgM can be detected as early as day 2 after infection and typically peaks on day 6 after infection, whereas virus-specific IgG usually becomes detectable from day 6 after infection.[54–56] We hypothesised that IgM produced during primary infection might be essential to control OROV replication. To test this hypothesis, we pooled sera harvested from WT mice on days 3–6 after infection and transferred 100 μL to *Rag1*$^{-/-}$ mice on the day of viral challenge. WT sera harvested on days 3–5 after infection delayed the development of neurological disease and death ($p < 0.001$ versus WT sera harvested on day 6, log-rank test with Bonferroni correction). In contrast, WT sera harvested on day 6 after infection protected *Rag1*$^{-/-}$ mice from OROV challenge, albeit in some cases with evidence of systemic viral replication (Fig. 4a–c). To establish the role of IgM in this phenomenon, we treated the protective serum samples with β-ME to chemically deplete IgM[57] before transfer to *Rag1*$^{-/-}$ mice. β-ME-treated sera lost protective activity against OROV challenge, and all recipient *Rag1*$^{-/-}$ mice succumbed to infection, with high viral loads in peripheral organs and the CNS (Fig. 4d–f). The efficacy of β-ME treatment was confirmed via ELISA and the FRNT (Fig. 4g–i).

MyD88 deletion in B cells modulates the antibody response against OROV

As the MyD88 signalling pathway in B cells was essential for restricting OROV pathogenesis and replication (Fig. 3), and neutralising antibodies inhibited the development of viral encephalitis as soon as day 6 after infection (Fig. 4), we determined whether MyD88 signalling in B cells modulated the production of antibodies against OROV. For this purpose, we quantified OROV-specific antibodies in serum samples harvested from WT and *CD19*-Cre^{+} *MyD88*^{fl} mice on days 6 and 14 after infection. Lower OROV-specific IgM titres with reduced avidity were found in *CD19*-Cre^{+} *MyD88*^{fl} mice compared with WT mice on day 6 after infection ($p < 0.001$ and $p < 0.05$, respectively, Mann–Whitney test with Bonferroni correction) (Fig. 5a–c). *CD19*-Cre^{+} *MyD88*^{fl} mice also exhibited lower OROV-specific IgG titres on day 14 after infection than WT mice ($p < 0.0001$, Mann–Whitney test with Bonferroni correction) (Fig. 5b). Moreover, IgG antibody avidities were lower in *CD19*-Cre^{+} *MyD88*^{fl} mice compared with WT mice on day 14 after infection, but this was not significant (Fig. 5d).

We then evaluated the neutralising capacity of heat-inactivated serum samples using the FRNT. Higher neutralising antibody titres were detected in WT mice compared with *CD19*-Cre^{+} *MyD88*^{fl} mice on day 14 after infection ($p < 0.01$, Mann–Whitney test with Bonferroni correction) (Fig. 5f–h). Moreover, *CD19*-Cre^{+} *MyD88*^{fl} mice exhibited neutralising antibody titres that were similar to those of naive WT mice, both on day 6 and on day 14 after infection (Fig. 5g and h). MyD88 deficiency in B cells reduced the neutralisation potency of OROV-specific IgM antibodies by 1.21 $\log_{10}$ on day 6 after infection and the neutralisation potency of OROV-specific IgG antibodies by 3.17 $\log_{10}$ on day 14 after infection compared with WT mice ($p < 0.001$ and $p < 0.0001$, respectively, Mann–Whitney test with Bonferroni correction) (Fig. 5e). *CD19*-Cre^{+} *MyD88*^{fl} mice that died also produced lower titres of neutralising antibodies than *CD19*-Cre^{+} *MyD88*^{fl} mice that survived throughout the course of infection, but this was not significant (Fig. 5i).

To determine the biological relevance of these findings, we pooled sera harvested from *CD19*-Cre^{+} *MyD88*^{fl} mice on days 6 or 14 after infection and transferred 100 μL to *Rag1*$^{-/-}$ mice on the day of viral challenge. Recipient *Rag1*$^{-/-}$ mice developed neurological disease, with high viral loads in peripheral organs and the CNS, and died from the infection (Fig. 5j–l). These collective

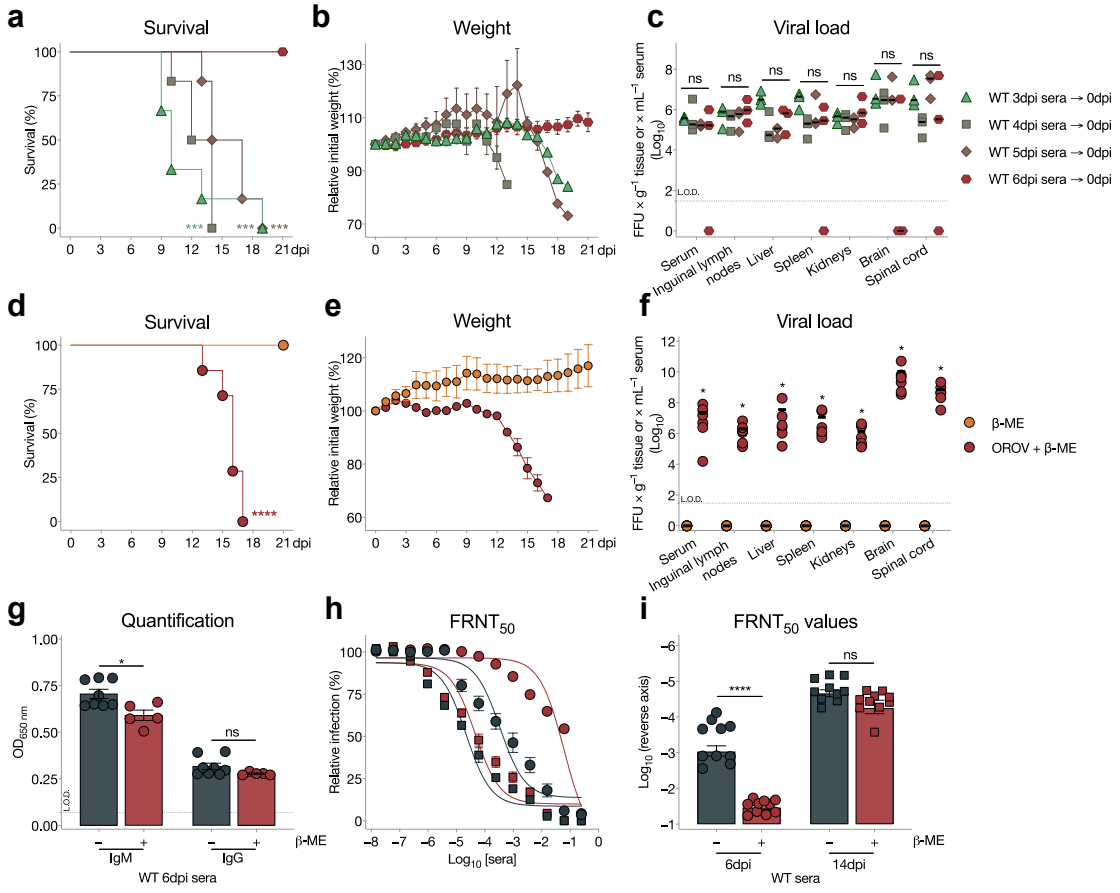

***Fig. 4:* Mortality, weight loss, and viral loads for *Rag1*$^{-/-}$ mice and IgM responses after OROV infection.** (a) Survival and (b) weight of *Rag1*$^{-/-}$ mice inoculated on the day of OROV challenge with sera harvested from WT mice 3–6 days post-infection (dpi) (coloured numbers, $n = 6$ per group). (c) Viral loads in serum and tissues from mice in (a, b) measured via focus-forming assay (coloured numbers, $n = 6$ per group). (d) Survival and (e) weight of *Rag1*$^{-/-}$ mice inoculated on the day of mock manipulation (orange, $n = 5$) or OROV challenge (red, $n = 7$) with β-ME-treated sera harvested from WT mice on day 6 post-infection. (f) Viral loads in serum and tissues from mice in (d, e) measured via focus-forming assay ($n = 5$ for mock manipulation, $n = 7$ for OROV challenge). Statistical differences were assessed using a log-rank test with Bonferroni correction (a, d) or the Kruskal–Wallis test with Dunn's post-hoc test across all tissue samples (c, f). ***$p < 0.001$, ****$p < 0.0001$, ns = not significant. Symbols represent death events (a, d), mean ± SEM (b, e), or individual viral loads (c, f), and lines represent mean values (c, f). Data were pooled from at least three independent experiments. (g) Anti-OROV ELISA and (h) FRNT analyses of sera harvested from WT mice on days 6 or 14 post-infection before (grey, $n = 10$) and after treatment with β-ME (red, $n = 5$). (i) $FRNT_{50}$ values for individual mice in (g, h) ($n = 10$ per group). Statistical differences were assessed using the Mann–Whitney test with Bonferroni correction (g, i). *$p < 0.05$, ****$p < 0.0001$, ns = not significant. Symbols represent individual mice (g, i) or mean ± SEM (h), bars represent mean ± SEM (g, i), and lines represent three-parameter log-logistic regression curves for relative infection per dilution (h). Data were pooled from at least three independent experiments. L.O.D. = limit of detection.

results indicated that MyD88 signalling in B cells was required for the optimal production of neutralising antibodies against OROV during primary infection.

MyD88 signalling is required for the development and maintenance of B cell subsets during OROV infection

To better understand the impaired antibody response generated by B cells lacking MyD88 expression, we used flow cytometry to immunophenotype B cell subsets from the spleens of WT and *CD19*-Cre^{+} *MyD88*^{fl} mice (Supplemental Fig. S5). We observed increased numbers of B220^{hi} cells, follicular B cells, and memory B cells ($p < 0.01$ for each subset, Mann–Whitney test with Bonferroni correction) (Fig. 6a, b, e, h, j) and reduced numbers of B220^{hi} CD138^{int} CD38^{+} plasmablasts (PBs) in *CD19*-Cre^{+} *MyD88*^{fl} mice relative to WT mice on day 6 after infection ($p < 0.01$, Mann–Whitney test with Bonferroni correction) (Fig. 6a, b, k). *CD19*-Cre^{+} *MyD88*^{fl} mice also exhibited reduced

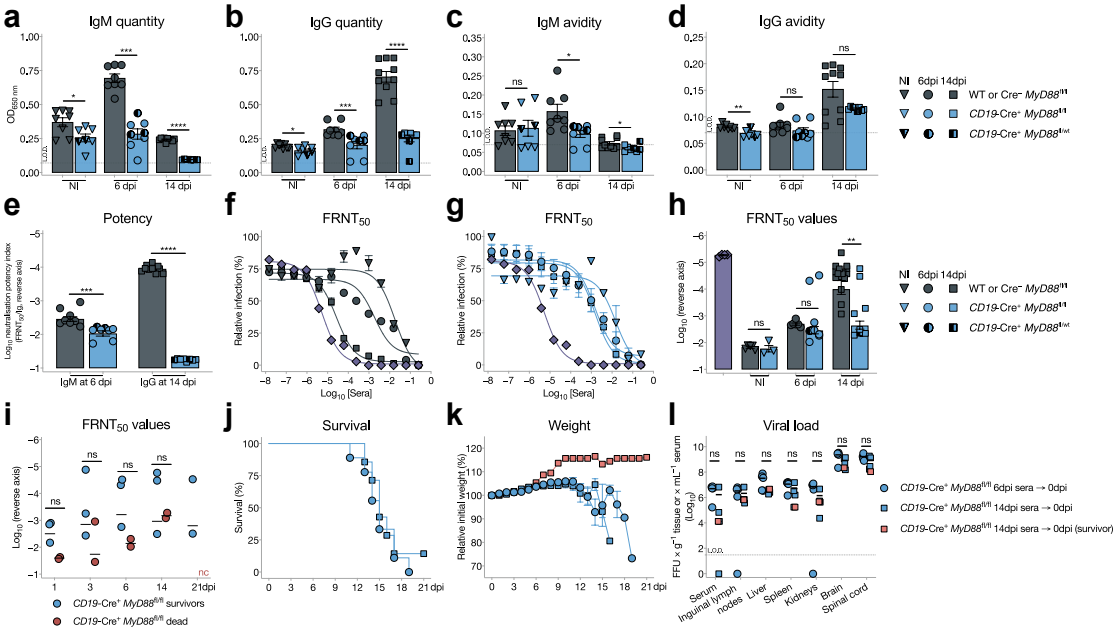

***Fig. 5:* Antibody responses in mice with *MyD88*-deficient B cells during OROV infection.** (a, b) Quantification and (c, d) avidity of OROV-specific IgM (a, c) and IgG isotypes (b, d) in serum samples (10-fold dilution) from WT mice (grey, $n = 8$ per condition/time point) and *CD19*-Cre^{+} *MyD88*^{fl} mice (blue, $n = 8$ per condition/time point) after mock manipulation (NI = noninfected) or at the indicated days post-infection (dpi) with 10^5 FFU of OROV. (e) Neutralisation potency index (log $FRNT_{50}$/Ig) of serum samples from WT mice and *CD19*-Cre^{+} *MyD88*^{fl} mice ($n = 8$ for 6 dpi and $n = 10$ for 14 dpi). Statistical differences were assessed using the Mann–Whitney test with Bonferroni correction (a–e). *$p < 0.05$, **$p < 0.01$, ***$p < 0.001$, ****$p < 0.0001$, ns = not significant. Symbols represent individual mice, and bars represent mean ± SEM (a–e). (f–h) FRNT analysis of sera harvested from (f) WT mice (grey, $n = 6$ for NI, $n = 6$ for 6 dpi, and $n = 16$ for 14 dpi) and (g) *CD19*-Cre^{+} *MyD88*^{fl} mice (blue, $n = 3$ for NI, $n = 8$ for 6 dpi, and $n = 8$ for 14 dpi) after mock manipulation or at the indicated days post-infection, with (h) $FRNT_{50}$ values for individual WT mice (grey, $n = 5$ for NI, $n = 6$ for 6 dpi, and $n = 16$ for 14 dpi) and *CD19*-Cre^{+} *MyD88*^{fl} mice (blue, $n = 3$ for NI, $n = 7$ for 6 dpi, and $n = 7$ for 14 dpi). Ascitic fluid (anti-OROV) was used as a positive control (purple). Statistical differences were assessed using the Mann–Whitney test with Bonferroni correction (h–i). **$p < 0.01$, ns = not significant. Symbols represent mean ± SEM (f, g) or individual mice (h), lines represent three-parameter log-logistic regression curves for relative infection per dilution (f, g), and bars represent mean ± SEM (h). (i) $FRNT_{50}$ values for individual *CD19*-Cre^{+} *MyD88*^{fl} mice that survived (blue, $n = 3$) or succumbed to the infection (red, $n = 2$). Statistical differences were assessed using the Mann–Whitney test with Bonferroni correction (i). ns = not significant. Symbols represent individual mice, and lines represent mean values (i). nc = noncollected sample. (j) Survival and (k) weight of *Rag1*$^{-/-}$ mice inoculated on the day of OROV challenge with sera harvested from *CD19*-Cre^{+} *MyD88*^{fl} mice on day 6 (circles, $n = 9$) or day 14 post-infection (squares, $n = 7$). (l) Viral loads in serum and tissues from mice in (j, k) measured via focus-forming assay ($n = 5$ per group). Statistical differences were assessed using a log-rank test with Bonferroni correction (j) or the Kruskal–Wallis test with Dunn's post-hoc test across all tissue samples (l). ns = not significant. Symbols represent death events (j), mean ± SEM (k), or individual viral loads (l), and lines represent mean values (l). L.O.D. = limit of detection.

numbers of B220^{int} cells, MZB cells, B220^{hi} CD138^{int} CD38^{+} PBs, and B220^{int} CD138^{+} PBs relative to WT mice on day 14 after infection ($p < 0.01$ for B220^{int} cells, MZB cells, and B220^{hi} CD138^{int} CD38^{+} PBs and $p < 0.05$ for B220^{int} CD138^{+} PBs, Mann–Whitney test with Bonferroni correction) (Fig. 6a, b, d, g, k, l). No significant differences in cellularity among B cell subsets were observed between uninfected groups of mice (Fig. 6c–m). Cell frequencies adhered to a similar pattern (Supplemental Fig. S6). It was also notable that *CD19*-Cre^{+} *MyD88*^{fl} mice with a clinical score of 2 on day 6 and a clinical score of 3 on day 14 after infection showed signs of neurological disease and exhibited decreased cellularity across almost all B cell subsets analysed at each time point (Fig. 6c–m). These observations suggested that MyD88 signalling in B cells was essential for the development and maintenance of B cell subsets during OROV infection.

Marginal zone B cells are required for effective control of OROV infection

To integrate our findings and determine the correlates of protection against OROV, we incorporated the values for IgM and IgG quantity, avidity, and neutralisation potency (index and $FRNT_{50}$), brain viral loads, mortality, and the cellularity of B cell populations from WT

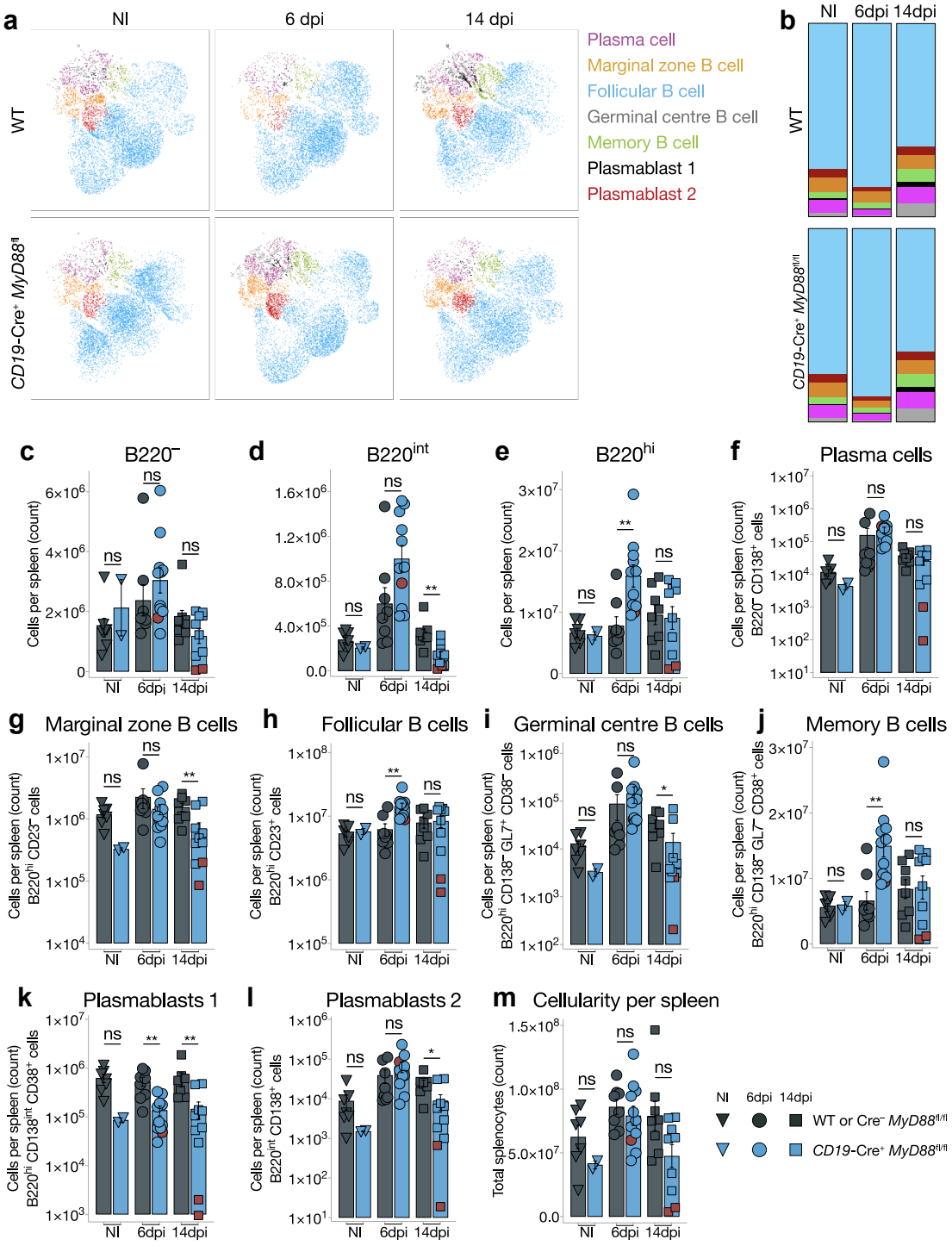

***Fig. 6:* B cell subset development and maintenance in *MyD88*-deficient mice during OROV infection.** (a) Uniform Manifold Approximation and Projection (UMAP) representation of splenic $CD3^-$ $Gr1^-$ $F4/80^-$ lymphocytes from WT mice (grey, *n* = 8 per condition/time point) and *CD19*-Cre^+ *MyD88*^{fl} mice (blue, *n* = 3 for noninfected [NI] and *n* = 8 at each time point) after mock manipulation or at days 6 or 14 post-infection (dpi) with 10^5 FFU of OROV. (b) B cell subset frequencies among splenic $CD3^-$ $Gr1^-$ $F4/80^-$ lymphocytes from (a). (c–m) B cell numbers per spleen for the indicated subsets from WT mice (grey, *n* = 8 per condition/time point) and *CD19*-Cre^+ *MyD88*^{fl} mice (blue, *n* = 3 for NI and *n* = 8 at each time point) after mock manipulation or at days 6 or 14 post-infection with 10^5 FFU of OROV. B cell subsets were

and *CD19*-Cre^{+} *MyD88*^{fl} mice into a FAMD. The categorical variable of genotype clearly segregated individuals into two groups, with 37.4% of the variance in Dim-1 and 21% of the variance in Dim-2, together with the categorical variable of mortality associated with the *CD19*-Cre^{+} *MyD88*^{fl} genotype (Fig. 7a). The quantitative variables of high IgM and IgG quantity and avidity, MZB cell and B220^{hi} CD138^{int} CD38^{+} PB cellularity, and total cellularity were associated with the WT genotype, whereas low neutralisation potency indices and $FRNT_{50}$ values and high viral loads in the CNS were associated with the *CD19*-Cre^{+} *MyD88*^{fl} genotype (Fig. 7b). The variables with contributions above the uniform average in Dim-1 were the cellularity of B220^{hi} cells, B220^{int} cells, B220^{-} cells, plasma cells, germinal centre B cells, B220^{int} CD138^{+} PBs, MZB cells, follicular B cells, and total cellularity (Fig. 7c). The variables with contributions above the uniform average in Dim-2 were genotype, neutralisation potency (indices and $FRNT_{50}$ values), IgG quantity, and B220^{hi} CD138^{int} CD38^{+} PB cellularity (Fig. 7d). Tracking the contributions of variables across all dimensions further suggested that MZB cells were central to the divergent response between WT and *CD19*-Cre^{+} *MyD88*^{fl} mice, followed by genotype, mortality, distinct populations of PBs, viral loads in the CNS, and antibody activity (Fig. 7e).

To corroborate these findings, we adoptively transferred MZB cells isolated from naive WT or *CD19*-Cre^{+} *MyD88*^{fl} mice via flow cytometry to *Rag1*$^{-/-}$ or *CD19*-Cre^{+} *MyD88*^{fl} mice on the day before OROV challenge. *CD19*-Cre^{+} *MyD88*^{fl} mice that received *CD19*-Cre^{+} *MyD88*^{fl} MZB cells remained proportionately vulnerable to disease, and all *Rag1*$^{-/-}$ mice that received *CD19*-Cre^{+} *MyD88*^{fl} MZB cells died from the infection ($p < 0.01$ versus WT MZB cells, log-rank test with Bonferroni correction) (Fig. 7f). In contrast, *CD19*-Cre^{+} *MyD88*^{fl} mice that received WT MZB cells were fully protected from disease, and some *Rag1*$^{-/-}$ mice that received WT MZB cells remarkably also survived the challenge (Fig. 7f). Of note, higher systemic titres of neutralising antibodies were detected in *CD19*-Cre^{+} *MyD88*^{fl} mice that received MZB cells from WT versus *CD19*-Cre^{+} *MyD88*^{fl} mice ($p < 0.01$, Mann–Whitney test with Bonferroni correction) (Fig. 7g and h).

Collectively, these findings demonstrated that a lack of MyD88 signalling in B cells impaired the development of lineage-defined subsets, including MZB cells, resulting in diminished neutralising antibody titres and limited control of OROV infection.

Discussion

Mechanisms of innate immunity, typically involving dendritic cells, macrophages, and other myeloid cells,[58–61] restrict many viral infections and synergise with adaptive immune responses, including B cell-mediated antibody production, to generate durable antiviral protection. All immune cells can recognise viral RNA via innate sensors, such as TLRs and other pattern recognition receptors (PRRs). Among the various molecules involved in intracellular signalling via PRRs, MyD88 is an essential adaptor protein recruited by IL-1R and several TLRs, such as TLR4, TLR7, TLR8, and TLR9[47,62–68] After activation via TLR7 and TLR9, MyD88 interacts with E3 ubiquitin ligase, TRAF6, and IFN regulatory factors, such as IRF5, altering gene expression.[69] MyD88 signalling in B cells is thought to be essential for T cell-dependent antibody responses, mainly due to enhanced production of germinal centre-dependent IgGs.[32,70,71]

We found previously that *Irf5*$^{-/-}$ mice progressed to encephalitis with lower titres of neutralising antibodies than WT mice after OROV infection.[28] IRF5 is associated with B cell maturation via the regulation of Blimp-1 (PRDM1).[31] However, these protective B cell responses seemed to control OROV infection independently of T cell activation, as TCRβδ mice were resistant to infection and displayed no signs of neurological injury. In contrast, *Rag1*$^{-/-}$ and μMT mice were vulnerable to OROV infection, developing neurological disease with microglial activation and high viral loads in the CNS. These observations also highlighted the neurotropic nature of OROV.[40,72–74]

Our initial hypothesis to explain how B cells could restrict OROV infection via a T cell-independent mechanism implicated the type I IFN response.[26,27,75] However, *CD19*-Cre^{+} *Ifnar*^{fl} mice were resistant to OROV infection. Although OROV can downregulate IFN signalling *in vitro*,[76] the type I IFN response in patients with OROV fever is not related to the timing of seroconversion,[77] whereas in some other infections, IFN signalling in B cells is required for the development of antiviral humoral immunity.[78] Direct viral infection as a means of B cell activation also seemed unlikely, given that B cells minimally express low-density lipoprotein receptor-related protein 1 (LRP1),[79,80] a known entry receptor for

evaluated via flow cytometry as (c) B220^{-}, (d) B220^{int}, (e) B220^{hi}, (f) B220^{-} CD138^{+} (plasma cells), (g) B220^{hi} CD23^{-} (marginal zone B cells), (h) B220^{hi} CD23^{+} (follicular B cells), (i) B220^{hi} CD138^{-} GL7^{+} CD38^{-} (germinal centre B cells), (j) B220^{hi} CD138^{-} GL7^{-} CD38^{+} (memory B cells), (k) B220^{hi} CD138^{int} CD38^{+} (plasmablasts 1), and (l) B220^{int} CD138^{+} (plasmablasts 2), alongside total cellularity (m). Statistical differences were assessed using the Mann–Whitney test with Bonferroni correction. *$p < 0.05$, **$p < 0.01$, ns = not significant. Symbols represent individual mice, and bars represent mean ± SEM. Red symbols indicate samples harvested from mice with clinical scores of 2 (at 6 dpi) or 3 (at 14 dpi).

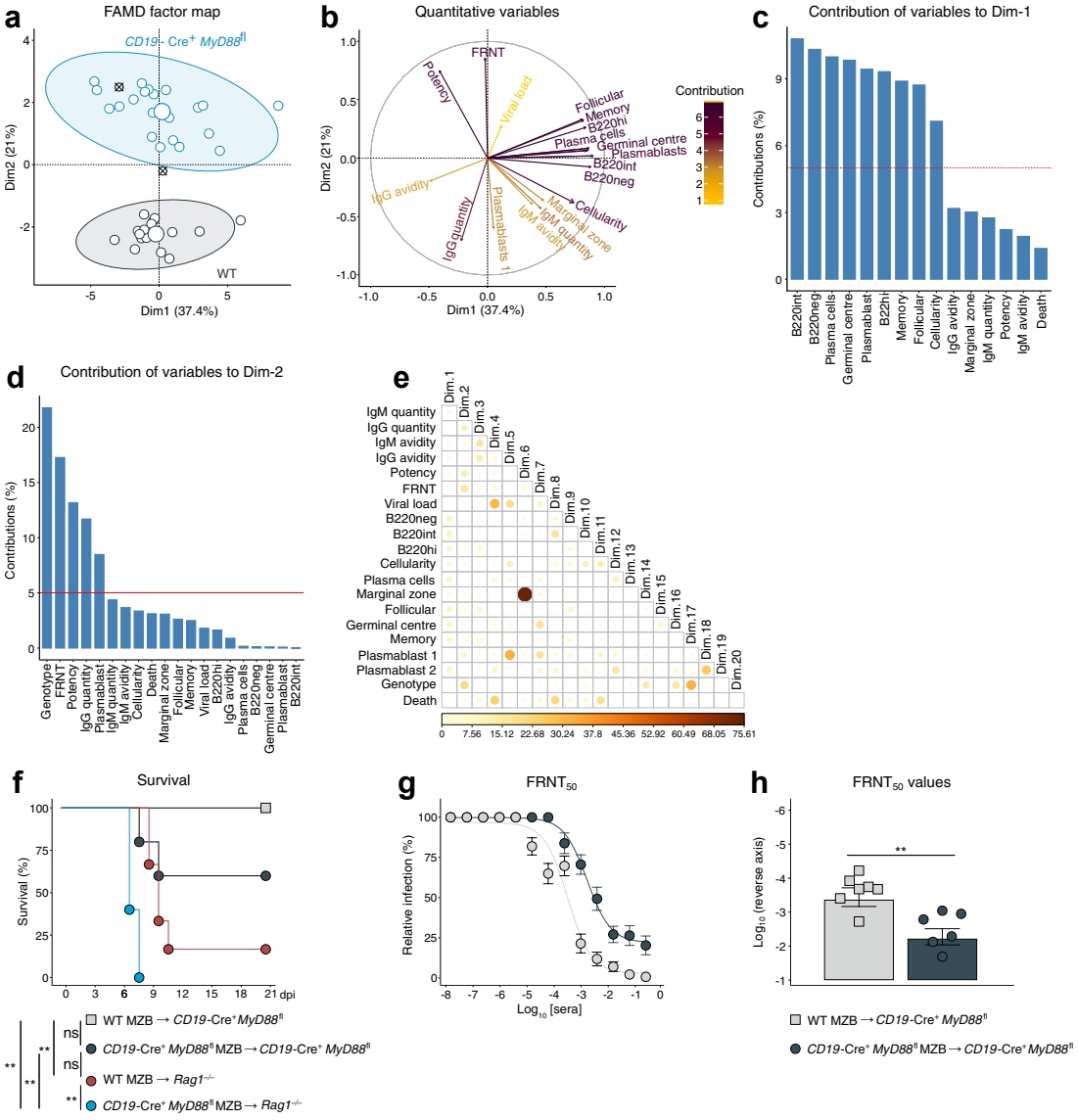

***Fig. 7*: The role of marginal zone B cells during OROV infection.** Factor analysis of mixed data (FAMD) using mouse genotypes, IgM and IgG quantity, avidity, and neutralisation potency (indices and $FRNT_{50}$ values), viral loads in brains, death events, and the cellularity of B cell subsets. (a) FAMD factor map showing the categorical variable of genotype for WT mice (n = 8 for noninfected [NI], n = 8 for 6 dpi, and n = 10 for 14 dpi) and *CD19*-Cre$^+$ *MyD88*^{fl} mice (n = 7 for NI, n = 11 for 6 dpi, and n = 10 for 14 dpi). Colour-coded circles represent individual mice, white circles represent group centroids, and crossed circles represent the categorical variables of live (middle) and death events (top). (b) Quantitative variables are represented by arrows coloured to indicate relative contribution in each case (key) for WT mice (n = 8 for NI, n = 8 for 6 dpi, and n = 10 for 14 dpi) and *CD19*-Cre$^+$ *MyD88*^{fl} mice (n = 7 for NI, n = 11 for 6 dpi, and n = 10 for 14 dpi). (c, d) The percent contribution of each variable to (c) Dim-1 and (d) Dim-2 for WT mice (n = 8 for NI, n = 8 for 6 dpi, and n = 10 for 14 dpi) and *CD19*-Cre$^+$ *MyD88*^{fl} mice (n = 7 for NI, n = 11 for 6 dpi, and n = 10 for 14 dpi). The red line indicates the expected average value for a uniform contribution. (e) Correlation matrix colour-coded for percent contribution and variables for each dimension for WT mice (n = 8 for NI, n = 8 for 6 dpi, and n = 10 for 14 dpi) and *CD19*-Cre$^+$ *MyD88*^{fl} mice (n = 7 for NI, n = 11 for 6 dpi, and n = 10 for 14 dpi). Data were pooled from at least three independent experiments. Plasmablasts 1 = B220^{hi} CD138^{int} CD38$^+$ cells, plasmablasts 2 = B220^{int} CD138$^+$ cells. (f) Survival of *Rag1*$^{-/-}$ mice (red circles, n = 6) and *CD19*-Cre$^+$ *MyD88*^{fl} mice (light grey squares, n = 6) after adoptive transfer of WT MZB cells or *Rag1*$^{-/-}$ mice (blue circles, n = 5) and *CD19*-Cre$^+$ *MyD88*^{fl} mice (dark grey circles, n = 5) after adoptive transfer of *CD19*-Cre$^+$ *MyD88*^{fl} MZB cells over 21 days post-infection (dpi) with 10^5 FFU of OROV. Statistical differences were assessed using a log-rank test with Bonferroni correction (f). $^{**}p < 0.01$, ns = not significant (f). Symbols represent death events (f). (g) FRNT analysis of sera from *CD19*-Cre$^+$ *MyD88*^{fl} mice at terminal harvest after adoptive transfer of WT MZB cells (light grey, n = 6) or *CD19*-Cre$^+$ *MyD88*^{fl} MZB cells (dark grey, n = 5) during OROV infection as

OROV.[81] In contrast, *CD19*-Cre^{+} *MyD88*^{fl} mice succumbed to OROV infection, despite the induction of a classical inflammatory profile in terms of chemokine and cytokine release.

Natural antibodies produced by B1 cells in a T cell-independent manner via MyD88 signalling can contribute to pathogen-specific immunity.[51,82–88] We found that naive WT sera did not protect *Rag1*$^{-/-}$ mice from OROV challenge, making this scenario unlikely. However, these findings were not sufficient to exclude a role for natural antibodies in the pathogenesis of OROV, given the lack of full serological reconstitution.

A much clearer protective role has been established for neutralising antibodies in the context of several primary arboviral infections. For example, antibody evasion mechanisms contribute to the pathogenesis of Chikungunya virus and Dengue virus, and an early IgM response is required to restrict the dissemination of West Nile virus into the CNS.[57,89–91] We found that passive transfer of neutralising OROV-specific IgM produced by WT mice within 6 days of infection could protect *Rag1*$^{-/-}$ mice from a lethal dose of OROV. Sera harvested from WT mice at the peak of the neutralising antibody response (day 14 post-infection) also protected *Rag1*$^{-/-}$ mice when administered up to 3 days after OROV challenge. An important implication of these findings is that antibody-based therapies would likely need to be administered within a narrow time window to prevent the development of OROV-mediated neurological disease.[92]

Although some studies have shown that MyD88 is important for pathogen-specific and vaccine-induced immunity,[68,78,93–95] relatively little is known about this pathway in the context of arboviral infections, including OROV. We found that mice lacking MyD88 expression in B cells produced lower amounts of neutralising antibodies than WT mice after OROV infection. These serum-derived antibodies also exhibited weaker avidity and potency profiles in *CD19*-Cre^{+} *MyD88*^{fl} versus WT mice. In line with these findings, passive serum transfer from *CD19*-Cre^{+} *MyD88*^{fl} mice failed to protect *Rag1*$^{-/-}$ mice against OROV challenge. However, some *CD19*-Cre^{+} *MyD88*^{fl} mice survived the infection and produced higher titres of neutralising antibodies than *CD19*-Cre^{+} *MyD88*^{fl} mice that succumbed to the infection, potentially reflecting immune pathway redundancy, mosaicism, and/or a lack of protein loss in the Cre recombinase system.[96–99] Additional studies will be required to resolve this discrepancy and dissect the role of highly avid neutralising antibodies as mediators of immune protection against OROV.

Neurologically sick *CD19*-Cre^{+} *MyD88*^{fl} mice exhibited altered B cell subset cellularity after OROV infection, indicating a key role for MyD88 in B cell development[62,68] and antiviral immunity. T cell-independent antigens for B cell responses are classified into type I antigens, such as lipopolysaccharide (LPS), CpG sites in DNA, and polyinosinic-polycytidylic acid (poly I:C), and type II antigens, which are often carbohydrate structures.[100,101] The spike glycoproteins of bunyaviruses[10] can act as type II antigens in a T cell-independent manner. MZB cells are major responders to lipid antigens but can also recognise type II antigens and blood-borne pathogens, subsequently producing large amounts of IgM and/or differentiating into plasma cells.[71,101–103] Our immunophenotypic analysis of B cell populations showed that MZB cells and PBs expanded numerically in WT mice after OROV infection. In contrast, B220^{int} cells and B220^{hi} cells predominated in *CD19*-Cre^{+} *MyD88*^{fl} mice, likely reflecting impaired B cell maturation.[104] The relative paucity of MZB cells in *CD19*-Cre^{+} *MyD88*^{fl} mice could feasibly impact type II antigen responses,[101,102,105,106] such as those targeting glycoproteins derived from OROV. MZB cells were also described as the primary discriminator between WT and *CD19*-Cre^{+} *MyD88*^{fl} mice in our FAMD. Of note, IgM^{+} IgD^{+} CD27^{+} B cell numbers are reduced in patients with IRAK4 or MyD88 deficiency, impairing T cell-independent IgM responses to type I antigens from encapsulated bacteria, such as *Streptococcus pneumoniae*.[107]

B cell proliferation and plasma cell formation can be intrinsically promoted by signals delivered via TLRs,[62] which are compromised in mice lacking MyD88. In line with this paradigm, adoptively transferred MZB cells from WT but not *CD19*-Cre^{+} *MyD88*^{fl} mice protected *CD19*-Cre^{+} *MyD88*^{fl} and *Rag1*$^{-/-}$ mice against OROV. PB numbers were also reduced in *CD19*-Cre^{+} *MyD88*^{fl} mice, especially those with clinical scores of 2 or 3, further indicating a link between antibody production and protection against OROV. Moreover, the process of somatic mutation that occurs in germinal centres to generate high-affinity antibody responses[108,109] was likely diminished in neurologically sick *CD19*-Cre^{+} *MyD88*^{fl} mice, which harboured fewer germinal centre B cells and mounted weaker antibody responses compared with WT mice. Genotype-specific associations between the antibody response and perturbations among B cell subsets were further confirmed via FAMD. These data linked the role of MyD88 signalling in B cell differentiation with the quality of the antibody response against OROV.[62]

in (f). Symbols represent mean ± SEM, and lines represent three-parameter log-logistic regression curves for relative infection per dilution (g). (h) $FRNT_{50}$ values for individual mice in (g) after adoptive transfer of WT MZB cells (light grey, $n = 6$) or *CD19*-Cre^{+} *MyD88*^{fl} MZB cells (dark grey, $n = 5$). Statistical differences were assessed using the Mann–Whitney test (h). $^{**}p < 0.01$. Symbols represent individual mice, and bars represent mean ± SEM (h). MZB = marginal zone B.

It is important to highlight the limitations of our study. First, we did not dissect the upstream or downstream mechanisms by which MyD88 regulates antibody secretion, which could inform the precise molecular basis of immune protection against OROV. Second, we did not investigate the clonal repertoire or the transcriptional profile of B cells lacking MyD88, which could feasibly distinguish between intrinsic signals required for B cell development and the nature of the peripheral immune response. Third, we did not use inducible systems to modulate developing B cells in other strains of mice, and we did not titrate the infectious dose of OROV, both of which could help refine our understanding of specific antibody production. Fourth, we did not blind investigators to mouse group allocations during experimentation, which could bias data collection. Fifth, we did not extend our investigations to humans or other strains of OROV, which are potentially more relevant to public health. Sixth, we did not undertake a comprehensive evaluation of antigen-specific memory B cells over time, either in the periphery or in the bone marrow. These latter investigations will be required to understand the maintenance of antibody-mediated immunity, which is critical for durable protection against subsequent infections with OROV.

In summary, our findings delineate a mechanism by which the early innate and adaptive immune functions of B cells, including MZB cells, operate synergistically to restrict the neuropathogenesis of OROV, an emerging arthropod-borne virus in Latin America (Fig. 8). Our results draw particular attention to the importance of the adaptor protein MyD88, which regulates B cell differentiation and the production of

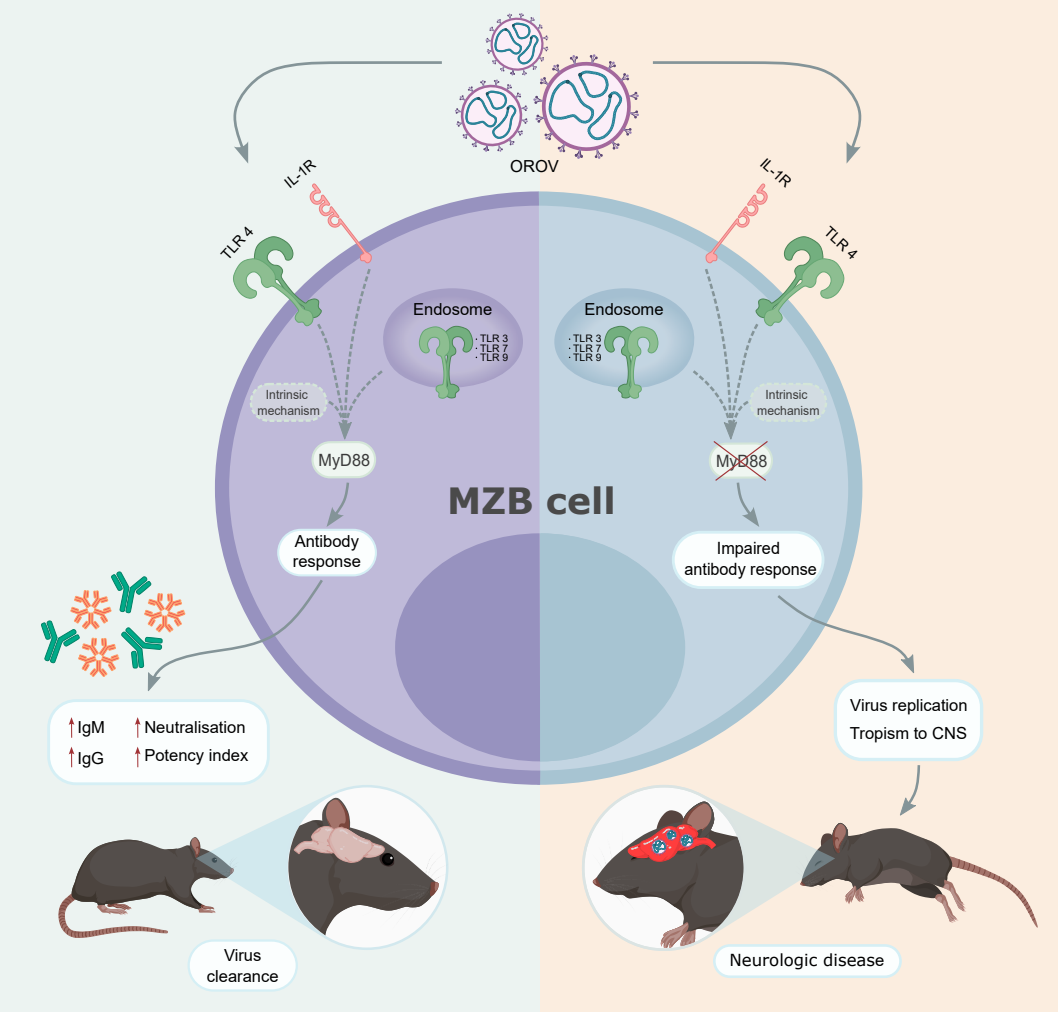

***Fig. 8:* Interpretation of the study.** Early antibody responses produced mainly by MZB cells in a MyD88-dependent manner restrict viral replication and spread to the central nervous system, protecting mice from encephalitis and subsequent death after infection with OROV.

neutralising antibodies during primary infection, enabling viral clearance and preventing the disease manifestations of OROV. As such, our work could inform the development of antibody treatment strategies and vaccines to attenuate the pathogenesis and spread of OROV, which is currently an emerging pathogen of global concern.

Contributors

Conceptualisation: DATT, ELVS, and JLPM. Methodology: DATT, PLP, BBPS, CLS, AV, JF, MCM, MRA, KBdS, NSB, GFdS, LDC, MAF, SPM, PPB, VAM, XH, and GPM. Investigation: DATT, PLP, BBPS, CLS, AV, JF, MCM, MRA, KBdS, NSB, GFdS, LDC, MAF, SPM, PPB, VAM, XH, and GPM. Writing — original draft: DATT and JLPM. Writing — review and editing: DATT, PMMMV, FG, PL, MARV, GPM, REM, CAF, WMdS, ASF, DAP, MSD, ELVS, and JLPM. Visualisation: DATT, FG, MARV, GPM, REM, CAF, WMdS, ASF, DAP, MSD, ELVS, and JLPM. Funding acquisition: WMdS, MSD, ELVS, and JLPM. Resources; PMMMV, MAV, DATT, ASF, MSD, ELVS, and JLPM. Supervision: ELVS and JLPM. Data access and verification: DATT, ELVS, and JLPM. All authors contributed intellectually and approved the final version of the manuscript for publication.

Data sharing statement

All raw data generated during the course of this study have been deposited in the Unicamp Research Data Repository (https://doi.org/10.25824/redu/YVNDUS). Any data reported in this paper that is not available in the Unicamp Research Data Repository can be shared by the lead contacts upon reasonable request and subject to institutional approval.

Declaration of interests

MSD is an advisor or consultant for Moderna, Ocugen, Topspin Therapeutics, IntegerBio, MacroGenics, Inbios, Akagera Medicines, Merck, Bavarian Nordic, GlaxoSmithKline, and Vir Biotechnology. MSD has received unrelated funding via sponsored research agreements from Moderna, Emergent BioSolutions, Bavarian Nordic, and Vir Biotechnology. DAP has received unrelated funding via competitive awards from the Medical Research Council, the Open Medicine Foundation, the PolyBio Research Foundation, and the National Institute for Health Research.

Acknowledgements

We are grateful for financial support from the São Paulo Research Foundation (FAPESP) awarded to ELVS and JLPM (2016/00194-8 and 2017/11931-6) and to PLP, CLS, JF, KBdS, GFdS, and SPM (2017/22062-9, 2017/26908-0, 2018/10224-7, 2018/13645-3, 2020/02159-0, and 2020/02448-2), the National Council for Scientific and Technological Development (CNPq) awarded to ELVS and JLPM (304377/2021-0 and 309971/2023-3) and to DATT and MCM (141844/2019-1 and 421724/2017-0), and the Coordination for the Improvement of Higher Education Personnel (CAPES) awarded to MRA and PPB (88887.356527/2019-00 and 88887.661921/2022-00). BBPS was supported by the Unicamp Research Affairs Office (01-P-109/2022). ELVS was supported by the PIPAE from the University of São Paulo (2021.1.10424.1.9). WMdS was supported by a Wellcome Trust Digital Technology Development Award (Climate-Sensitive Infectious Disease Modelling) (226075/Z/22/Z). We also thank Lucas Miguel de Carvalho, Ph.D., from São Francisco University and Alina Malyutina, M. Sc., from the University of Helsinki for statistical supervision, Renata Chaves Albuquerque from the University of São Paulo and staff at the Life Sciences Core Facility (LaCTAD) at Unicamp for assistance with analytical cell biology and flow cytometry, and Julia Forato, B.Sc., for design of the study interpretation figure. This study was also supported by the National Institute of Science and Technology on Photonics Applied to Cell Biology (INFABIC, Unicamp) (FAPESP 2014/50938-8 and CNPq 465699/2014-6).

Appendix A. Supplementary data

Supplementary data related to this article can be found at https://doi.org/10.1016/j.ebiom.2025.105815.

References

1 Pinheiro FD, Pinheiro M, Bensabath G, Causey OR, Shope RE. Epidemia de vírus Oropouche em Belém. *Rev Ser Esp Saude Pub*. 1962;12:15–23.
2 Anderson CR, Spence L, Downs WG, Aitken TH. Oropouche virus: a new human disease agent from Trinidad, West Indies. *Am J Trop Med Hyg*. 1961;10:574–578. https://doi.org/10.4269/ajtmh.1961.10.574.
3 Romero-Alvarez D, Escobar LE. Oropouche fever, an emergent disease from the Americas. *Microbes Infect*. 2018;20:135–146. https://doi.org/10.1016/j.micinf.2017.11.013.
4 Baisley KJ, Watts DM, Munstermann LE, Wilson ML. Epidemiology of endemic Oropouche virus transmission in upper Amazonian Peru. *Am J Trop Med Hyg*. 1998;59:710–716. https://doi.org/10.4269/ajtmh.1998.59.710.
5 Ministério da Saúde. Oropouche. https://www.gov.br/saude/pt-br/assuntos/saude-de-a-a-z/o/oropouche/painel-epidemiologico. Accessed April 25, 2025.
6 Scachetti GC, Forato J, Claro IM, et al. Re-emergence of Oropouche virus between 2023 and 2024 in Brazil: an observational epidemiological study. *Lancet Infect Dis*. 2025;25:166–175. https://doi.org/10.1016/S1473-3099(24)00619-4.
7 Lancet Infectious Diseases. Oropouche fever, the mysterious threat. *Lancet Infect Dis*. 2024;24:935. https://doi.org/10.1016/S1473-3099(24)00516-4.
8 Pan American Health Organization. Epidemiological alert oropouche in the region of the americas. https://www.paho.org/en/documents/epidemiological-alert-oropouche-region-americas-9-may-2024. Accessed April 25, 2025.
9 Vasconcelos HB, Nunes MRT, Casseb LMN, et al. Molecular epidemiology of Oropouche virus, Brazil. *Emerg Infect Dis*. 2011;17:800–806. https://doi.org/10.3201/eid1705.101333.
10 Elliott RM. Orthobunyaviruses: recent genetic and structural insights. *Nat Rev Microbiol*. 2014;12:673–685. https://doi.org/10.1038/nrmicro3332.
11 International Committee on Taxonomy of Viruses. Orthobunyavirus oropoucheense. https://ictv.global/taxonomy/taxondetails?taxnode_id=202200124. Accessed April 25, 2025.
12 Naveca FG, Almeida TAP de, Souza V, et al. Human outbreaks of a novel reassortant Oropouche virus in the Brazilian Amazon region. *Nat Med*. 2024;30:3509–3521. https://doi.org/10.1038/s41591-024-03300-3.
13 Travassos da Rosa JF, de Souza WM, Pinheiro FP, et al. Oropouche virus: clinical, epidemiological, and molecular aspects of a neglected Orthobunyavirus. *Am J Trop Med Hyg*. 2017;96:1019–1030. https://doi.org/10.4269/ajtmh.16-0672.
14 Mourão MPG, Bastos Mde S, de Figueiredo RMP, et al. Arboviral diseases in the Western Brazilian Amazon: a perspective and analysis from a tertiary health & research center in Manaus, State of Amazonas. *Rev Soc Bras Med Trop*. 2015;48(Suppl 1):20–26. https://doi.org/10.1590/0037-8682-0133-2013.
15 Pinheiro FP, Travassos da Rosa AP, Travassos da Rosa JF, Bensabath G. An outbreak of Oropouche virus disease in the vicinity of Santarem, Para, Brazil. *Tropenmed Parasitol*. 1976;27:213–223.
16 Pinheiro FP, Travassos da Rosa AP, Travassos da Rosa JF, et al. Oropouche virus. I. A review of clinical, epidemiological, and ecological findings. *Am J Trop Med Hyg*. 1981;30:149–160.
17 Rosa AP, Rodrigues SG, Nunes MR, Magalhães MT, Rosa JF, Vasconcelos PF. Outbreak of oropouche virus fever in Serra Pelada, municipality of Curionópolis, Pará, 1994. *Rev Soc Bras Med Trop*. 1996;29:537–541. https://doi.org/10.1590/s0037-86821996000600002.
18 de Souza Luna LK, Rodrigues AH, Santos RIM, et al. Oropouche virus is detected in peripheral blood leukocytes from patients. *J Med Virol*. 2017;89:1108–1111. https://doi.org/10.1002/jmv.24722.
19 Ribeiro Amorim M, Cornejo Pontelli M, Fabiano de Souza G, et al. Oropouche virus infects, persists and induces IFN response in human peripheral blood mononuclear cells as identified by RNA PrimeFlow™ and qRT-PCR assays. *Viruses*. 2020;12:785. https://doi.org/10.3390/v12070785.

20 Ministério da Saúde. Ministério da Saúde informa caso de anomalia congênita associada à Oropouche. https://www.gov.br/saude/pt-br/canais-de-atendimento/sala-de-imprensa/notas-a-imprensa/2024/ministerio-da-saude-informa-caso-de-anomalia-congenita-associada-a-oropouche. Accessed April 25, 2025.
21 Ministério da Saúde. Ministério da Saúde confirma um óbito fetal por Oropouche em Pernambuco. https://www.gov.br/saude/pt-br/assuntos/noticias/2024/agosto/saude-confirma-um-obito-fetal-por-oropouche-em-pernambuco. Accessed April 25, 2025.
22 Ministério da Saúde. Ministério da Saúde confirma dos óbitos por Oropouche no país. https://www.gov.br/saude/pt-br/canais-de-atendimento/sala-de-imprensa/notas-a-imprensa/2024/ministerio-da-saude-confirma-dois-obitos-por-oropouche-no-pais. Accessed April 25, 2025.
23 Bastos Mde S, Figueiredo LTM, Naveca FG, et al. Identification of Oropouche orthobunyavirus in the cerebrospinal fluid of three patients in the Amazonas, Brazil. *Am J Trop Med Hyg*. 2012;86:732–735. https://doi.org/10.4269/ajtmh.2012.11-0485.
24 Pinheiro FP, Rocha AG, Freitas RB, et al. Meningitis associated with Oropouche virus infections. *Rev Inst Med Trop Sao Paulo*. 1982;24:246–251.
25 Vernal S, Martini CCR, da Fonseca BAL. Oropouche virus-associated aseptic meningoencephalitis, southeastern Brazil. *Emerg Infect Dis*. 2019;25:380–382. https://doi.org/10.3201/eid2502.181189.
26 Ivashkiv LB, Donlin LT. Regulation of type I interferon responses. *Nat Rev Immunol*. 2014;14:36–49. https://doi.org/10.1038/nri3581.
27 McNab F, Mayer-Barber K, Sher A, Wack A, O'Garra A. Type I interferons in infectious disease. *Nat Rev Immunol*. 2015;15:87–103. https://doi.org/10.1038/nri3787.
28 Proenca-Modena JL, Hyde JL, Sesti-Costa R, et al. Interferon-regulatory factor 5-dependent signaling restricts Orthobunyavirus dissemination to the central nervous system. *J Virol*. 2015;90:189–205. https://doi.org/10.1128/JVI.02276-15.
29 Wang L, Zhu Y, Zhang N, et al. The multiple roles of interferon regulatory factor family in health and disease. *Signal Transduct Target Ther*. 2024;9:282. https://doi.org/10.1038/s41392-024-01980-4.
30 Fabié A, Mai LT, Dagenais-Lussier X, Hammami A, van Grevenynghe J, Stäger S. IRF-5 promotes cell death in CD4 T cells during chronic infection. *Cell Rep*. 2018;24:1163–1175. https://doi.org/10.1016/j.celrep.2018.06.107.
31 Lien C, Fang C-M, Huso D, Livak F, Lu R, Pitha PM. Critical role of IRF-5 in regulation of B-cell differentiation. *Proc Natl Acad Sci USA*. 2010;107:4664–4668. https://doi.org/10.1073/pnas.0911193107.
32 Pasare C, Medzhitov R. Control of B-cell responses by Toll-like receptors. *Nature*. 2005;438:364–368. https://doi.org/10.1038/nature04267.
33 van Kuppeveld FJ, Johansson KE, Galama JM, et al. Detection of mycoplasma contamination in cell cultures by a mycoplasma group-specific PCR. *Appl Environ Microbiol*. 1994;60:149–152. https://doi.org/10.1128/aem.60.1.149-152.1994.
34 R Core Team. R: a language and environment for statistical computing. https://www.r-project.org/. Accessed April 25, 2025.
35 Lê S, Josse J, Husson F. FactoMineR: an R package for multivariate analysis. *J Stat Softw*. 2008;25:1–18. https://doi.org/10.18637/jss.v025.i01.
36 Kassambara A, Mundt F. factoextra: extract and visualize the results of multivariate data analyses. https://cran.r-project.org/web/packages/factoextra/index.html. Accessed April 25, 2025.
37 Ritz C, Baty F, Streibig JC, Gerhard D. Dose-response analysis using R. *PLoS One*. 2015;10:e0146021. https://doi.org/10.1371/journal.pone.0146021.
38 McInnes L, Healy J, Saul N, Großberger L. UMAP: uniform Manifold approximation and projection. *J Open Source Softw*. 2018;3:861. https://doi.org/10.21105/joss.00861.
39 Van Gassen S, Callebaut B, Van Helden MJ, et al. FlowSOM: using self-organizing maps for visualization and interpretation of cytometry data. *Cytometry A*. 2015;87:636–645. https://doi.org/10.1002/cyto.a.22625.
40 Santos RI, Almeida MFP, Paula FE, et al. Experimental infection of suckling mice by subcutaneous inoculation with Oropouche virus. *Virus Res*. 2012;170:25–33. https://doi.org/10.1016/j.virusres.2012.07.006.
41 Proenca-Modena JL, Sesti-Costa R, Pinto AK, et al. Oropouche virus infection and pathogenesis are restricted by MAVS, IRF-3, IRF-7, and type I interferon signaling pathways in nonmyeloid cells. *J Virol*. 2015;89:4720–4737. https://doi.org/10.1128/JVI.00077-15.
42 Mombaerts P, Iacomini J, Johnson RS, Herrup K, Tonegawa S, Papaioannou VE. RAG-1-deficient mice have no mature B and T lymphocytes. *Cell*. 1992;68:869–877. https://doi.org/10.1016/0092-8674(92)90030-g.
43 Kitamura D, Roes J, Kühn R, Rajewsky K. A B cell-deficient mouse by targeted disruption of the membrane exon of the immunoglobulin μ chain gene. *Nature*. 1991;350:423–426. https://doi.org/10.1038/350423a0.
44 Mombaerts P, Clarke AR, Rudnicki MA, et al. Mutations in T-cell antigen receptor genes α and β block thymocyte development at different stages. *Nature*. 1992;360:225–231. https://doi.org/10.1038/360225a0.
45 Diamond MS, Gale M Jr. Cell-intrinsic innate immune control of West Nile virus infection. *Trends Immunol*. 2012;33:522–530. https://doi.org/10.1016/j.it.2012.05.008.
46 Figueiredo CM, Neris RL da S, Gavino-Leopoldino D, et al. Mayaro virus replication restriction and induction of muscular inflammation in mice are dependent on age, type-I interferon response, and adaptive immunity. *Front Microbiol*. 2019;10:2246. https://doi.org/10.3389/fmicb.2019.02246.
47 McCarthy MK, Reynoso GV, Winkler ES, et al. MyD88-dependent influx of monocytes and neutrophils impairs lymph node B cell responses to Chikungunya virus infection via Irf5, Nos2 and Nox2. *PLoS Pathog*. 2020;16:e1008292. https://doi.org/10.1371/journal.ppat.1008292.
48 de Almeida LA, Carvalho NB, Oliveira FS, et al. MyD88 and STING signaling pathways are required for IRF3-mediated IFN-β induction in response to *Brucella abortus* infection. *PLoS One*. 2011;6:e23135. https://doi.org/10.1371/journal.pone.0023135.
49 Warner N, Núñez G. MyD88: a critical adaptor protein in innate immunity signal transduction. *J Immunol*. 2013;190:3–4. https://doi.org/10.4049/jimmunol.1203103.
50 Ochsenbein AF, Pinschewer DD, Sierro S, Horvath E, Hengartner H, Zinkernagel RM. Protective long-term antibody memory by antigen-driven and T help-dependent differentiation of long-lived memory B cells to short-lived plasma cells independent of secondary lymphoid organs. *Proc Natl Acad Sci USA*. 2000;97:13263–13268. https://doi.org/10.1073/pnas.230417497.
51 Ochsenbein AF, Fehr T, Lutz C, et al. Control of early viral and bacterial distribution and disease by natural antibodies. *Science*. 1999;286:2156–2159. https://doi.org/10.1126/science.286.5447.2156.
52 Alter G, Ottenhoff THM, Joosten SA. Antibody glycosylation in inflammation, disease and vaccination. *Semin Immunol*. 2018;39:102–110. https://doi.org/10.1016/j.smim.2018.05.003.
53 Law M, Hangartner L. Antibodies against viruses: passive and active immunization. *Curr Opin Immunol*. 2008;20:486–492. https://doi.org/10.1016/j.coi.2008.06.005.
54 Lum F-M, Teo T-H, Lee WWL, Kam Y-W, Rénia L, Ng LFP. An essential role of antibodies in the control of Chikungunya virus infection. *J Immunol*. 2013;190:6295–6302. https://doi.org/10.4049/jimmunol.1300304.
55 Devito C, Ellegård R, Falkeborn T, et al. Human IgM monoclonal antibodies block HIV-transmission to immune cells in cervicovaginal tissues and across polarized epithelial cells in vitro. *Sci Rep*. 2018;8:10180. https://doi.org/10.1038/s41598-018-28242-y.
56 Shen C, Zhang M, Chen Y, et al. An IgM antibody targeting the receptor binding site of influenza B blocks viral infection with great breadth and potency. *Theranostics*. 2019;9:210–231. https://doi.org/10.7150/thno.28434.
57 Diamond MS, Shrestha B, Marri A, Mahan D, Engle M. B cells and antibody play critical roles in the immediate defense of disseminated infection by West Nile encephalitis virus. *J Virol*. 2003;77:2578–2586. https://doi.org/10.1128/jvi.77.4.2578-2586.2003.
58 Bowen JR, Quicke KM, Maddur MS, et al. Zika virus antagonizes type I interferon responses during infection of human dendritic cells. *PLoS Pathog*. 2017;13:e1006164. https://doi.org/10.1371/journal.ppat.1006164.
59 Liu Y, Gordesky-Gold B, Leney-Greene M, Weinbren NL, Tudor M, Cherry S. Inflammation-induced, STING-dependent autophagy restricts Zika virus infection in the Drosophila brain. *Cell Host Microbe*. 2018;24:57–68.e3. https://doi.org/10.1016/j.chom.2018.05.022.

60 de Castro-Jorge LA, de Carvalho RVH, Klein TM, et al. The NLRP3 inflammasome is involved with the pathogenesis of Mayaro virus. *PLoS Pathog*. 2019;15:e1007934. https://doi.org/10.1371/journal.ppat.1007934.

61 Carnec X, Baize S, Reynard S, et al. Lassa virus nucleoprotein mutants generated by reverse genetics induce a robust type I interferon response in human dendritic cells and macrophages. *J Virol*. 2011;85:12093–12097. https://doi.org/10.1128/JVI.00429-11.

62 Tian M, Hua Z, Hong S, et al. B cell-intrinsic MyD88 signaling promotes initial cell proliferation and differentiation to enhance the germinal center response to a virus-like particle. *J Immunol*. 2018;200:937–948. https://doi.org/10.4049/jimmunol.1701067.

63 Schoenemeyer A, Barnes BJ, Mancl ME, et al. The interferon regulatory factor, IRF5, is a central mediator of Toll-like receptor 7 signaling. *J Biol Chem*. 2005;280:17005–17012. https://doi.org/10.1074/jbc.M412584200.

64 Chiang H-S, Liu HM. The molecular basis of viral inhibition of IRF- and STAT-dependent immune responses. *Front Immunol*. 2018;9:3086. https://doi.org/10.3389/fimmu.2018.03086.

65 Dinarello CA. The IL-1 family of cytokines and receptors in rheumatic diseases. *Nat Rev Rheumatol*. 2019;15:612–632. https://doi.org/10.1038/s41584-019-0277-8.

66 Oliveira A-C, Gomes-Neto JF, Barbosa C-HD, et al. Crucial role for T cell-intrinsic IL-18R-MyD88 signaling in cognate immune response to intracellular parasite infection. *Elife*. 2017;6:e30883. https://doi.org/10.7554/eLife.30883.

67 Thackray LB, Shrestha B, Richner JM, et al. Interferon regulatory factor 5-dependent immune responses in the draining lymph node protect against West Nile virus infection. *J Virol*. 2014;88:11007–11021. https://doi.org/10.1128/JVI.01545-14.

68 Kang S-M, Yoo D-G, Kim M-C, et al. MyD88 plays an essential role in inducing B cells capable of differentiating into antibody-secreting cells after vaccination. *J Virol*. 2011;85:11391–11400. https://doi.org/10.1128/JVI.00080-11.

69 Balkhi MY, Fitzgerald KA, Pitha PM. Functional regulation of MyD88-activated interferon regulatory factor 5 by K63-linked polyubiquitination. *Mol Cell Biol*. 2008;28:7296–7308. https://doi.org/10.1128/mcb.00662-08.

70 Heer AK, Shamshiev A, Donda A, et al. TLR signaling fine-tunes anti-influenza B cell responses without regulating effector T cell responses. *J Immunol*. 2007;178:2182–2191. https://doi.org/10.4049/jimmunol.178.4.2182.

71 Khan AQ, Chen Q, Wu Z-Q, Paton JC, Snapper CM. Both innate immunity and type 1 humoral immunity to *Streptococcus pneumoniae* are mediated by MyD88 but differ in their relative levels of dependence on Toll-like receptor 2. *Infect Immun*. 2005;73:298–307. https://doi.org/10.1128/IAI.73.1.298-307.2005.

72 Almeida GM, Souza JP, Mendes ND, et al. Neural infection by Oropouche virus in adult human brain slices induces an inflammatory and toxic response. *Front Neurosci*. 2021;15:674576. https://doi.org/10.3389/fnins.2021.674576.

73 Rodrigues AH, Santos RI, Arisi GM, et al. Oropouche virus experimental infection in the golden hamster (Mesocrisetus auratus). *Virus Res*. 2011;155:35–41. https://doi.org/10.1016/j.virusres.2010.08.009.

74 Santos RI, Bueno-Júnior LS, Ruggiero RN, et al. Spread of Oropouche virus into the central nervous system in mouse. *Viruses*. 2014;6:3827–3836. https://doi.org/10.3390/v6103827.

75 Ali S, Mann-Nüttel R, Schulze A, Richter L, Alferink J, Scheu S. Sources of type I Interferons in infectious immunity: plasmacytoid dendritic cells not always in the driver's seat. *Front Immunol*. 2019;10:778. https://doi.org/10.3389/fimmu.2019.00778.

76 Geddes VEV, Brustolini OJB, Cavalcante LT de F, et al. Common dysregulation of innate immunity pathways in human primary astrocytes infected with Chikungunya, Mayaro, Oropouche, and Zika viruses. *Front Cell Infect Microbiol*. 2021;11:641261. https://doi.org/10.3389/fcimb.2021.641261.

77 de Oliveira E, Azevedo Rdo SS, Coelho-Dos-Reis JG, et al. IFN-α as a time-sensitive biomarker during Oropouche virus infection in early and late seroconverters. *Sci Rep*. 2019;9:17924. https://doi.org/10.1038/s41598-019-54223-w.

78 Fink K, Lang KS, Manjarrez-Orduno N, et al. Early type I interferon-mediated signals on B cells specifically enhance antiviral humoral responses. *Eur J Immunol*. 2006;36:2094–2105. https://doi.org/10.1002/eji.200635993.

79 Baldarelli RM, Smith CL, Ringwald M, Richardson JE, Bult CJ. Mouse genome informatics group. Mouse genome informatics: an integrated knowledgebase system for the laboratory mouse. *Genetics*. 2024;227:iyae031. https://doi.org/10.1093/genetics/iyae031.

80 Thul PJ, Åkesson L, Wiking M, et al. A subcellular map of the human proteome. *Science*. 2017;356:eaal3321. https://doi.org/10.1126/science.aal3321.

81 Schwarz MM, Price DA, Ganaie SS, et al. Oropouche orthobunyavirus infection is mediated by the cellular host factor Lrp1. *Proc Natl Acad Sci USA*. 2022;119:e2204706119. https://doi.org/10.1073/pnas.2204706119.

82 Baumgarth N. How specific is too specific? B-cell responses to viral infections reveal the importance of breadth over depth. *Immunol Rev*. 2013;255:82–94. https://doi.org/10.1111/imr.12094.

83 Holodick NE, Rodríguez-Zhurbenko N, Hernández AM. Defining natural antibodies. *Front Immunol*. 2017;8:872. https://doi.org/10.3389/fimmu.2017.00872.

84 Ochsenbein AF, Zinkernagel RM. Natural antibodies and complement link innate and acquired immunity. *Immunol Today*. 2000;21:624–630. https://doi.org/10.1016/s0167-5699(00)01754-0.

85 Jayasekera JP, Moseman EA, Carroll MC. Natural antibody and complement mediate neutralization of influenza virus in the absence of prior immunity. *J Virol*. 2007;81:3487–3494. https://doi.org/10.1128/JVI.02128-06.

86 Baumgarth N, Herman OC, Jager GC, Brown L, Herzenberg LA, Herzenberg LA. Innate and acquired humoral immunities to influenza virus are mediated by distinct arms of the immune system. *Proc Natl Acad Sci USA*. 1999;96:2250–2255. https://doi.org/10.1073/pnas.96.5.2250.

87 Zhou Z-H, Zhang Y, Hu Y-F, Wahl LM, Cisar JO, Notkins AL. The broad antibacterial activity of the natural antibody repertoire is due to polyreactive antibodies. *Cell Host Microbe*. 2007;1:51–61. https://doi.org/10.1016/j.chom.2007.01.002.

88 Barr TA, Brown S, Mastroeni P, Gray D. B cell intrinsic MyD88 signals drive IFN-γ production from T cells and control switching to IgG2c. *J Immunol*. 2009;183:1005–1012. https://doi.org/10.4049/jimmunol.0803706.

89 Hawman DW, Fox JM, Ashbrook AW, et al. Pathogenic Chikungunya virus evades B cell responses to establish persistence. *Cell Rep*. 2016;16:1326–1338. https://doi.org/10.1016/j.celrep.2016.06.076.

90 Clapham HE, Rodriguez-Barraquer I, Azman AS, et al. Dengue virus (DENV) neutralizing antibody kinetics in children after symptomatic primary and postprimary DENV infection. *J Infect Dis*. 2016;213:1428–1435. https://doi.org/10.1093/infdis/jiv759.

91 Diamond MS, Sitati EM, Friend LD, Higgs S, Shrestha B, Engle M. A critical role for induced IgM in the protection against West Nile virus infection. *J Exp Med*. 2003;198:1853–1862. https://doi.org/10.1084/jem.20031223.

92 Goyal A, Cardozo-Ojeda EF, Schiffer JT. Potency and timing of antiviral therapy as determinants of duration of SARS-CoV-2 shedding and intensity of inflammatory response. *Sci Adv*. 2020;6:eabc7112. https://doi.org/10.1126/sciadv.abc7112.

93 Hou B, Saudan P, Ott G, et al. Selective utilization of Toll-like receptor and MyD88 signaling in B cells for enhancement of the antiviral germinal center response. *Immunity*. 2011;34:375–384. https://doi.org/10.1016/j.immuni.2011.01.011.

94 Upasani V, Rodenhuis-Zybert I, Cantaert T. Antibody-independent functions of B cells during viral infections. *PLoS Pathog*. 2021;17:e1009708. https://doi.org/10.1371/journal.ppat.1009708.

95 Rawlings DJ, Schwartz MA, Jackson SW, Meyer-Bahlburg A. Integration of B cell responses through Toll-like receptors and antigen receptors. *Nat Rev Immunol*. 2012;12:282–294. https://doi.org/10.1038/nri3190.

96 Nish S, Medzhitov R. Host defense pathways: role of redundancy and compensation in infectious disease phenotypes. *Immunity*. 2011;34:629–636. https://doi.org/10.1016/j.immuni.2011.05.009.

97 Fischer A, Rausell A. Primary immunodeficiencies suggest redundancy within the human immune system. *Sci Immunol*. 2016;1:eaah5861. https://doi.org/10.1126/sciimmunol.aah5861.

98 Turlo KA, Gallaher SD, Vora R, Laski FA, Iruela-Arispe ML. When Cre-mediated recombination in mice does not result in protein loss. *Genetics*. 2010;186:959–967. https://doi.org/10.1534/genetics.110.121608.

99 Heffner CS, Herbert Pratt C, Babiuk RP, et al. Supporting conditional mouse mutagenesis with a comprehensive cre characterization resource. *Nat Commun*. 2012;3:1218. https://doi.org/10.1038/ncomms2186.

100 Obukhanych TV, Nussenzweig MC. T-independent type II immune responses generate memory B cells. *J Exp Med*. 2006;203:305–310. https://doi.org/10.1084/jem.20052036.

101 Haniuda K, Nojima T, Ohyama K, Kitamura D. Tolerance induction of IgG^+ memory B cells by T cell-independent type II antigens. *J Immunol*. 2011;186:5620–5628. https://doi.org/10.4049/jimmunol.1100213.

102 Fagarasan S, Honjo T. T-Independent immune response: new aspects of B cell biology. *Science*. 2000;290:89–92. https://doi.org/10.1126/science.290.5489.89.

103 Li Y, Tang Y, Liu J, et al. Glia maturation factor-γ is involved in S1P-induced marginal zone B-cell chemotaxis and optimal IgM production to type II T-independent antigen. *Int Immunol*. 2022;34:35–43. https://doi.org/10.1093/intimm/dxab097.

104 Tachikawa S, Kawamura T, Kawamura H, et al. Appearance of $B220^{low}$ autoantibody-producing B-1 cells at neonatal and older stages in mice. *Clin Exp Immunol*. 2008;153:448–455. https://doi.org/10.1111/j.1365-2249.2008.03709.x.

105 Cerutti A, Cols M, Puga I. Marginal zone B cells: virtues of innate-like antibody-producing lymphocytes. *Nat Rev Immunol*. 2013;13:118–132. https://doi.org/10.1038/nri3383.

106 Zouali M, Richard Y. Marginal zone B-cells, a gatekeeper of innate immunity. *Front Immunol*. 2011;2:63. https://doi.org/10.3389/fimmu.2011.00063.

107 Maglione PJ, Simchoni N, Black S, et al. IRAK-4 and MyD88 deficiencies impair IgM responses against T-independent bacterial antigens. *Blood*. 2014;124:3561–3571. https://doi.org/10.1182/blood-2014-07-587824.

108 Tas JMJ, Mesin L, Pasqual G, et al. Visualizing antibody affinity maturation in germinal centers. *Science*. 2016;351:1048–1054. https://doi.org/10.1126/science.aad3439.

109 Liu D, Winer BY, Chou MY, et al. Dynamic encounters with red blood cells trigger splenic marginal zone B cell retention and function. *Nat Immunol*. 2024;25:142–154. https://doi.org/10.1038/s41590-023-01690-z.